Food Hydrocolloids 157 (2024) 110369

Contents lists available at ScienceDirect

Food Hydrocolloids

journal homepage: www.elsevier.com/locate/foodhyd

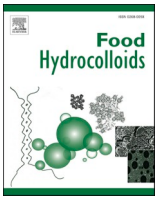

3D printing of plant-based fat inks towards manufacturing complex cellular agriculture products with fatty structures

Kristin Schüler [a,b], Diana M.C. Marques [a,b], Afonso Gusmão [a,b,c], Madalena Jabouille [a,b], Marco Leite [c], Joaquim M.S. Cabral [a,b], Paola Sanjuan-Alberte [a,b,**], Frederico Castelo Ferreira [a,b,*]

[a] Department of Bioengineering and Institute for Bioengineering and Biosciences, Instituto Superior Técnico, Universidade de Lisboa, Av. Rovisco Pais, 1049-001, Lisbon, Portugal
[b] Associate Laboratory i4HB—Institute for Health and Bioeconomy, Instituto Superior Técnico, Universidade de Lisboa, Av. Rovisco Pais, 1049-001, Lisbon, Portugal
[c] IDMEC, Instituto Superior Técnico, Universidade de Lisboa, Av. Rovisco Pais, 1049-001, Lisbon, Portugal

ARTICLE INFO

Keywords:
Plant-based biomaterials
Edible scaffolds
Fat-based ink
3D food printing
Cellular agriculture

ABSTRACT

3D printing of food is becoming increasingly popular and efforts are being directed at using this technology for cellular agriculture applications. Cell-based food products can be manufactured using 3D bioprinting processes combining different materials to obtain whole-meat structures including muscle, fat, and connective tissue. Therefore, there is a pressing need towards formulating inks that are printable at relatively low temperature levels (<40 °C) and printing pressures (<20 psi) exhibiting good printability and shape fidelity. Different fat-based inks based on sunflower oil (SFO), rapeseed oil (RSO) and olive oil (OO) were developed in this work fulfilling the aforementioned criteria. These inks presented comparable mechanical properties to animal tissues, more specifically to raw salmon fillet. Soy protein isolate (SPI) and κ-carrageenan (κ-CA) were used together with the different vegetable oils as emulsifiers and gelation agents, respectively. Additionally, carnauba wax (Cwax) was also incorporated into the above-mentioned vegetable oils to formulate oleogels (SFOwax). Biocompatibility and cell adhesion assays conducted with embryonic sea bass cells (DLEC, *Dicentrarchus labrax* Embryonic Cell Line) support their potential use in hybrid structures compatible with bioinks for 3D printing of food. Sensory properties of pure moulded fat-based samples and hybrids (moulded and printed) were evaluated in a double-compression test. In a second step, SFO and SFOwax were enriched with omega-3 oil, to improve their nutraceutical value. Finally, prototypes were developed using SFO40, confirming its great printability and suitability for the 3D printing of large and complex constructs. We present here for the first time a fully vegan, edible and 3D printable ink based on fat emulsions and oleogels compatible with fish cells for the development of 3D bioprinted food products.

1. Introduction

The emerging field of cellular agriculture offers a solution to the inner conflict of living sustainably while still enjoying nutrient-rich, delicious food. In a world with a growing population (United Nations-Department of Economic and Social Affairs and Population Division, 2019) there is an increasing demand for seafood and meat products. The consumption of these traditional animal protein sources is associated with several severe problems related to animal welfare, climate change and exceeded depletion of natural resources (Grossi, Goglio, Vitali, & Williams, 2019; Ramachandraiah, 2021; Tsuruwaka & Shimada, 2022; Tuomisto & Mattos, 2011).

Cellular agriculture on the other hand uses state-of-the-art technology combining biotechnology for cell culture with know-how in mechanical and materials engineering to provide more environmental-friendly alternative products containing animal proteins (K Handral,

* Corresponding author.Department of Bioengineering and Institute for Bioengineering and Biosciences, Instituto Superior Técnico, Universidade de Lisboa, Av. Rovisco Pais, 1049-001, Lisbon, Portugal.
** Corresponding author. Department of Bioengineering and Institute for Bioengineering and Biosciences, Instituto Superior Técnico, Universidade de Lisboa, Av. Rovisco Pais, 1049-001, Lisbon, Portugal.
E-mail addresses: paola.alberte@tecnico.ulisboa.pt (P. Sanjuan-Alberte), frederico.ferreira@tecnico.ulisboa.pt (F.C. Ferreira).

https://doi.org/10.1016/j.foodhyd.2024.110369
Received 20 March 2024; Received in revised form 7 June 2024; Accepted 26 June 2024
Available online 2 July 2024

Hua Tay, Wan Chan, & Choudhury, 2022; Rischer et al, 2020). One very important component of these is fat, due to its huge influence on the physical, sensory and energetic properties of food, particularly when developing structured products mimicking a fish or meat fillet (Listrat et al., 2016).

Additionally, plant-based fat alternatives for human consumption are being developed in a huge variety (Patel, Nicholson, & Marangoni, 2020; Wolfer, Acevedo, Prusa, Sebranek, & Tarté, 2018). Many of these formulations combine vegetable oils, such as corn oil or sunflower oil with plant-based proteins and/or carbohydrate systems. Here, starch (Shi, Zhang, & Bhandari, 2021) or algae-derived materials like κ-carrageenan (κ-CA) (Kamlow, Spyropoulos, & Mills, 2021; Tian et al., 2021) function as emulsifiers to allow the proper formation of stable emulsions (Hwang et al). However, these formulations are often optimized for moulding (Hou et al., 2022), and lack essential nutrients that can mainly or only be found in animal-derived products, e.g. the two omega-3 fatty acids docosahexaenoic acid (DHA) and eicosapentaenoic acid (EPA) (Watters, Edmonds, Sloss, Rosner, & Leung, 2012), or vitamin D3 (Schmid & Walther, 2013).

Plant- and cell-based products are often presented as unstructured products such as nuggets, burgers or sausages (Oh, Lee, Lee, & Lee, 2019; Patel et al., 2020; Wolfer et al., 2018). However, structured whole-meat products offer the advantage of increasing the consumer experience and acceptance (Dekkers, Boom, & van der Goot, 2018). Used in almost every industry sector nowadays including medicine, and automotive, among many others, three-dimensional (3D) extrusion printing is also an interesting additive manufacturing technology for shaping structured food products, creating layer-by-layer the desired structure. Due to its accuracy and precision, complex food structures can be developed by this method with tailored mechanical, nutritional and functional properties (Fahmy et al., 2021). 3D printing of food products could also improve the quality of life of patients suffering from dysphagia or other swallowing difficulties by improving the visual appearance and taste of food while preserving their safety by a precise control of texture (Kouzani et al., 2017; Zhao, Zhang, Chitrakar, & Adhikari, 2021).

In order to 3D print food products, the development of inks must meet certain requirements including an adequate viscosity that allows printing at tolerable pressures, while still providing high shape fidelity and stability of the printed constructs (K Handral et al., 2022; Zhao et al, 2021). First examples of 3D printed fat structures are known in shaping cake batter, and there are several works of fat-based and emulsion inks in 3D food printing of meat products (Guo et al., 2024; Jiménez-Colmenero et al., 2012; Paglarini et al., 2018; Shahbazi, Jäger, Chen, & Ettelaie, 2021) However, applications in the cellular agriculture sector and research on biocompatible fat-based food inks are limited (K Handral et al., 2022; Li et al., 2023), or the presented ink formulations are still using non-vegan materials, such as gelatine-based inks (Park et al., 2023), beeswax (Shi et al., 2021; Tian et al., 2021) or milk-derived whey protein isolate (Kamlow et al., 2021; Liu et al., 2019).

In this work, fat-based structures were developed based on fully vegan, biocompatible and edible materials by 3D printing. Inks' formulation consisted on vegetable oils, namely sunflower oil (SFO), rapeseed oil (RSO) and olive oil (OO) in combination with plant-based soy protein isolate (SPI) and κ- CA. SPI was used as a vegan, protein-rich amphiphilic emulsifier which shows improved digestibility, beneficial influence on human health as well as less allergic reaction compared to milk-derived products like whey protein isolate (Qin, Wang, & Luo, 2022; Santos-Hernández et al., 2020; Verduci et al., 2020). κ-CA was chosen as an environmental-friendly source of carbohydrate which is used in pristine form or as a blend with other animal- or plant-derived polysaccharides in many printable ink formulations due to its excellent biocompatibility, mechanical properties, good printability, and temperature-dependent gelation (Rhein-Knudsen, Ale, & Meyer, 2015; Yegappan, Selvaprithiviraj, Amirthalingam, & Jayakumar, 2018; Zia et al., 2017). Carnauba wax (Cwax) was also explored as a sustainable and vegan alternative to beeswax (Initiative For Responsible Carnauba, 2021).

To the best of our knowledge, this study presents, for the first time, plant-based and biocompatible inks with optimized printing conditions for precise printing results which can be potentially used as adipose inks in plant-based cellular agriculture products.

2. Materials and methods

2.1. Materials

Three different oils for the preparation of the emulsions were purchased at a local supermarket in Lisbon, Portugal, namely rapseed oil (RSO) (rapsolie, Salling Group), olive oil (OO) (Azeite dos nossos planaltos, Pingo Doce) and refined sunflower oil (SFO) (óleo de girassol, Continente). Carnauba wax (Cwax) was ordered from Plena natura (CAS 8015-86-9, Portugal). Kappa-carrageenan (κ-CA) was purchased from Sigma-Aldrich and used without further treatment. SPI powder was purchased at MP Biomedicals. Ultrapure water (MilliQ, Millipore) was used as solvent for SPI dispersion. Phosphate Buffered Saline (PBS) was purchased from Gibco.

Liquid omega-3 (ω-3) consisted on a vitadé liquid supplement containing vitamin D and Docosahexaenoic acid (DHA) with 2.000 μg and 4.000 mg 100 mL^{-1}, respectively (Inpharma SpA, Casorate Primo, Italy). Capsules of ω-3 consisted on a κ-CA shell containing approx. 600 μL of different vegetable oils and two of the essential ω-3 fatty acids: 150 mg Eicosapentaenoic acid (EPA) and 250 mg DHA per capsule, (MyVegan, The Hut.com Ltd. and Myprotein, Cheshire, England).

Fresh salmon fillets were purchased at a local supermarket (Pingo Doce, Portugal) and used to perform single and double compression tests on square-cut samples.

2.2. Preparation of emulsion inks

2.2.1. Preparation of SPI dispersion

Firstly, a 2 % (w/w) dispersion was prepared using SPI powder and ultrapure water and magnetically stirred at 50 °C for 5 h (pH 7). After hydration over night at 6 °C, ultrapure water was added to reach the final concentration of 1 % (w/w). Prior to its incorporation to the ink formulations, the SPI dispersion was stirred for 15 min at 50 °C.

2.2.2. Preparation of oleogel containing Cwax

The oleogels containing Cwax were prepared in a waterbath, where the SFO, RSO or OO were heated to around 90 °C. Then, 5 % (w/w) Cwax was added and left under magnetic stirring until melted and a homogenous liquid was obtained. The oleogels were cooled down to room temperature (RT) and stored for 24 h before use. Oleogels were heated to around 60 °C using a water bath prior to further use.

2.2.3. Preparation of final emulsion inks

SPI dispersion was preheated to 50 °C using magnetic stirring, and vegetable oil at 40 % (w/w) or preheated oleogel at 20 % (w/w) was added. Regarding the samples containing ω-3 oil, 5 % of the used SFO was replaced by ω-3 oil following the same protocol as described before.

The temperature was increased to 80 °C and the samples mixed for 30 min until obtaining an emulsion. Then, κ-CA was added at a concentration of 1.2 % (w/w) and continuously stirred for 2 h to obtain the final neutral inks (pH 7). Re-heating at the respective processing temperatures was performed when inks were not immediately used. The final concentrations of the different emulsion gels using SFO, RSO and OO can be seen in Table 1.

2.3. Sample preparation

2.3.1. Casted samples

Cylindrical moulds were 3D printed by fused deposit modelling using

Table 1
Ink formulations based on SFO, RSO and OO as well as formulations based on SFO including Omega-3 oil.

Name	Color code	Oil [w/w %]	ω-3 Oil [w/w %]	Cwax [w/w %]	SPI [w/w %]	κ-CA [w/w %]
SFOwax		19	-	1	0.8	1.2
SFO40		40	-	-	0.6	1.2
RSOwax		19	-	1	0.8	1.2
RSO40		40	-	-	0.6	1.2
OOwax		19	-	1	0.8	1.2
OO40		40	-	-	0.6	1.2
SFOwax-O3_vegan		18	1	1	0.8	1.2
SFO38-O3_vegan		38	2	-	0.6	1.2
SFOwax-O3_non-vegan		18	1	1	0.8	1.2
SFO38-O3_non-vegan		38	2	-	0.6	1.2

a Prusa i3 MK3S 3D extruder (PRUSA Research, Prague, Czech Republic) to support the ink during the casting process. These moulds (diameter of 9.5 mm and 10 mm in height) were produced with a PLA filament (1.75 mm, ivory white, smart materials 3d, Alcalá la Real, Jaén, Spain). During the casting process, the moulds were filled with the desired solution volume at 80 °C. Samples were left for approximately 10 min at RT and moulds were carefully removed.

2.3.2. 3D printing of simple structures

Printing was performed using a custom-made micro extrusion-based 3D printing system as described previously (Joung et al., 2018). Briefly, this system combines a three-axis Fisnar F4200N.2 dispensing robot (FISNAR, Germantown, WI, USA) with a pneumatic dispensing unit (DC100, FISNAR). Digital models were created and uploaded using the Fisnar RobotEdit software (FISNAR). 20-gauge dispensing tips of 0.5 mm inner diameter and 3 cc syringe barrels were used for all printing assays (FISNAR). Syringe barrel adaptors, end caps and pistons were also provided by FISNAR (QuantX).

For printability assessment, a 12 × 12 mm^2 mesh was printed as shown in Fig. S1a (Supporting Information). For stability and overall printing assessment, round towers with 10 mm of diameter and different number of layers (5, 10, 25) were printed using a distance between the layers of 0.3 mm at a printing speed of 10 mm/s (Figs. S1b and S1c). Printing pressure varied between 4 and 20 psi and temperature was kept at around 38 °C.

2.4. Characterisation of casted structures

2.4.1. Compression mechanical test

Uniaxial compression tests were performed on the casted structures using a 10 N load cell that was incorporated in a compression machine from Univert (CellScale Biomaterials Testing, Waterloo, ON, Canada). Prior to the experiment, samples (n = 5) were left in PBS overnight. The analysis was performed using a displacement rate of 3 mm min^{-1}. Stress-strain curves were calculated using the following formulas (Equations (1) and (2)):

$$\varepsilon\,[-] = \frac{\Delta L}{L_0} \qquad \text{[Eq. 1]}$$

were ΔL corresponds to the displacement in mm provided by the compression machine and L_0 to the initial height in mm.

$$\sigma\,\left[\mathrm{N\,mm^{-2}}\right] = \frac{F}{A} = \frac{4F}{\pi d^2} \qquad \text{Eq. 2}$$

where F corresponds to the force in N, measured by the compression machine; and A is the initial circular cross area of the specimen in mm^2, obtained by the initial diameter d in mm ($A = \frac{\pi}{4} d^2$).

Youngs' moduli were obtained from the linear strain region below 15 % of the stress-strain curves and from the linear strain region between 20 % and 40 %, see Equation (3).

$$\text{Young's modulus}\,\left[\mathrm{N\,mm^{-2}}\right] = \frac{\Delta\sigma}{\Delta\varepsilon} \qquad \text{Eq. 3}$$

where σ is stress in N mm^{-2} and strain ε is given dimensionless. Young's modulus, equivalent to the slope of the stress-strain curve in the related region, is given in N mm^{-2}, and was converted into kPa by the factor 10^3 (1 N mm^{-2} = 10^3 kPa).

2.4.2. Water content

To assess the water content, casted emulsion gels were weighted before and after drying at 40 °C over a period of 5 d. Measurements were taken on day 1, 2 and 5. The water content (%) was estimated using Equation (4):

$$\text{Water content}\,[\%] = \frac{W_0 - W_d}{W_0} * 100\% \qquad \text{Eq. 4}$$

where W_0 is the weight before drying and W_d after drying for 5 d. Measurements were performed in triplicate (n = 3).

2.4.3. Stability assessment of moulded structures

To assess stability of the different inks, casted samples (n = 3) were incubated in PBS at 4 °C and RT, respectively, for 21 d. During incubation, the PBS was carefully removed before the samples were weighted. Measurements were taken before submerging and after 1/24 d, 1/12 d, 3/4 d, 1 d, 2 d, 3 d, 4 d, 8 d, 14 d and 21 d. At day 4 and day 10, PBS was added to guarantee that the samples were kept hydrated. The weight loss was estimated using the following Equation (5):

$$\text{Weight loss}\,[\%] = \frac{W_s - W_0}{W_0} * 100\% \qquad \text{Eq. 5}$$

where W_0 is the weight prior to incubation and W_s relates to the weight during incubation.

2.5. Characterisation of fat-based inks

2.5.1. Rheological characterisation and temperature dependence

Rheological tests were conducted in triplicates (n = 3) using a MCR 92 modular compact rheometer from Anton Paar (Graz, Austria). A cone-plate geometry with 1° angle and a diameter of 50 mm was used. The sample volume was restricted to 500 μL to retain a measurement gap of 0.1 mm. To assess the temperature dependence and sol-gel transition temperature of the emulsion inks, samples were cooled from 50 to 27 °C

at a rate of 0.2 °C s^{-1}, while viscosity was constantly measured at a shear rate of 50 s^{-1}. Furthermore, time sweep tests were performed to evaluate the gelation kinetics and viscoelastic behaviour of the emulsion inks. Therefore, storage modulus (G′) and loss modulus (G″) were measured at a frequency of 1 Hz over 300 s, at 20 °C.

2.5.2. Thermal emulsion stability - measurement of cream index after freezing

Thermal emulsion stability was assessed adapting the protocol described elsewhere (Hong, Kim, & Lee, 2018). Briefly, 1–1.5 mL of the emulsion inks were transferred to 2 mL tubes at 80 °C and cooled to RT. Afterwards, samples underwent three freeze-thaw cycles, where each cycle corresponded to −20 °C for 23 h followed by heating to 90 °C for 15 min. After completing the cycles, the creaming index was assessed at RT using Equation (6) (Hong et al., 2018; McClements, 2007):

$$\text{Creaming index } [\%] = \frac{H_s}{H_T} * 100\% \quad \text{Eq. 6}$$

where H_s corresponds to the height of the serum layer and H_T to the total height of the emulsion sample (Fig. 1). Measurements were taken on images using ImageJ software (ImageJ 1.51f, National Institutes of Health, Bethesda, MD, USA) (n = 3).

2.5.3. Assessment of droplet size and distribution

Droplet size and distribution was assessed using printed meshes (12 × 12 mm^2) (Fig. S1a). The monolayer structures were examined instantly after printing using a Leica DMI3000B microscope (Leica Microsystems). Measurements were taken from three random areas (N = 3) of the size 100 x 100 μm^2. In each of these areas, a horizontal and vertical measurement was taken on five droplets to obtain an average droplet diameter using ImageJ software (n = 10).

2.5.4. Zeta potential

The emulsion stability was further assessed by determining the particle size and the surface potential using zeta potential (ζ-potential) measurements performed on a Zetasizer Nano SZ ZEN3600 (Malvern Panalytical, UK). Samples were diluted 1:100 (V/V) in deionised water to reduce the absorbance of laser light and multiple scattering, as described before by (Kamlow et al., 2021). All measurements were carried out at 25 °C and in triplicates (n = 3). Each value was recorded as the average of at least five measured data points.

2.6. Characterisation of ink printability

2.6.1. Printability assessment

One-layered meshes of 12 × 12 mm^2 containing nine pores (Fig. S1a) were printed to assess the printability of the different inks. The Printability factor (Pr) was determined using the formula from Equation (7) (Ouyang, Yao, Zhao, & Sun, 2016):

$$\text{Pr}[-] = \frac{L^2}{16\,A} \quad \text{Eq. 7}$$

where L is the perimeter of one pore in mm and A is the area of one pore in mm^2. Therefore, per mesh, nine measurements were performed based on images and evaluated using ImageJ. Values of Pr = 1 corresponded to perfectly squared printed pores, while higher values indicated cluttered pores, and lower values more circular pores (Ouyang et al., 2016). Using the same meshes, the line thickness was also compared to the theoretical needle tip diameter (0.5 mm) taking 12 measurements per 1-layered mesh.

2.6.2. Printability of multi-layered structures

Printability of multilayer structures was assessed using printed towers with 10 mm diameter and of 5, 10 and 25 layers height with 0.3 mm interlayer distance (Figs. S1b and S1c). The achieved height was assessed at 3 printed structures using the average of three points measured by a calliper (n = 9).

2.6.3. Two-week stability of printed structures

The long-term stability was conducted on one-layer printed meshes of 12 × 12 mm^2 (Fig. S1a). Structures were stored at RT in PBS and without PBS, respectively. Pictures were taken of triplicates right after printing, and after 1 d, 3 d, 7 d and 14 d. Printability was assessed using at least 10 measurements to show the printing stability over time (n = 10–15).

2.7. Cell culture, cell seeding and biocompatibility assessment

2.7.1. Cell culture and passaging of embryonic fish cells (DLEC)

An adherent embryonic fish cell line derived from European sea bass (Dicentrarchus labrax Embryonic Cell Line (DLEC)) was purchased from Kerafast (Boston, Massachusetts, USA) and proliferated as described elsewhere (Buonocore, Libertini, Prugnoli, Mazzini, & Scapigliati, 2006). Briefly, media was prepared using Leibovitz 15 medium (L-15 medium, Sigma Aldrich) containing 10 % (v/v) FBS, 1 % (v/v)

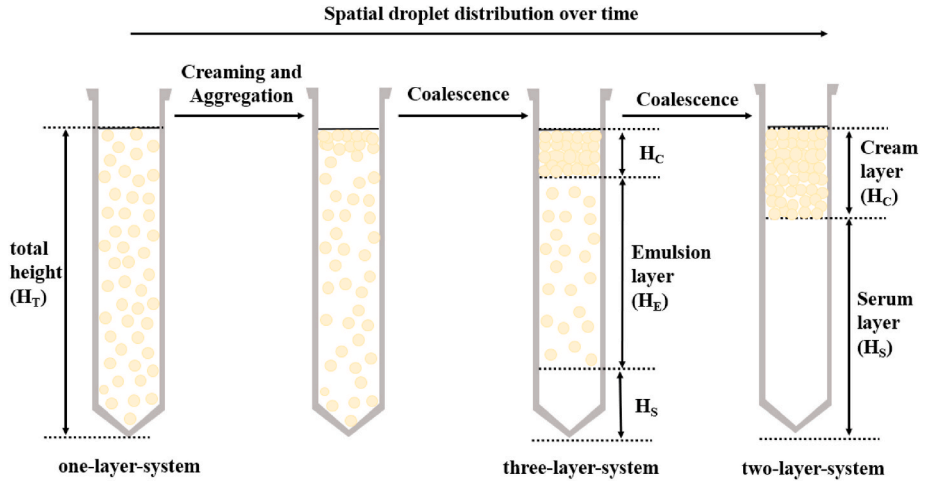

Fig. 1. Development of spatial droplet distribution over time from a monodisperse oil-in-water emulsion (one-layer system), over emulsion with early creaming to the top, and aggregation within the emulsion, to a three-layer-system with clearly separated cream layer to the top, emulsion layer in the middle and serum layer on the bottom until with further coalescence a two-layer-system develops where the cream layer is on top of the serum layer.

L-Glutamine (Sigma Aldrich), 1 % (v/v) Penicillin-Streptomycin (pen--strep, gibco) and 5 μL mL^{-1} of 3 M NaCl. The embryonic fish cells were incubated at 20 °C without CO_2. Media was exchanged every 2–3 d and passaging was done every 3–4 d, when confluent using Trypsin/EDTA (Passaging number 6 and 7, viability >90%).

2.7.2. Cytotoxicity evaluation

Firstly, moulded scaffolds (8–10 mm height, ~9.5 mm diameter, sterilised overnight in 5 % pen-strep in PBS) were placed on top of 90 % confluent DLEC cells on 24-well plates at a cell density of 40,000 cells mL^{-1} and incubated for 72 h. To prevent the scaffolds to float, cylindrical structures were printed and placed on top of the scaffolds to add weight ensuring a close contact with the cell population (Fig. S2a). Cell density was assessed after 72 h using a haemocytometer after Trypan blue (Thermo Fischer) staining (1:2). All cytotoxicity tests were performed in triplicates (n = 3).

Secondly, the bottom area of a 6-well plate was covered with the different emulsion inks and sterilised overnight in 5 % pen-strep PBS solution. Then, samples were washed with media and left at 4 °C for 96 h. Subsequently, the media in contact with the structures was collected and used to culture DLEC cells previously seeded onto a 24-well plate with a cell density of 20,000 cells mL^{-1} (n = 3). Cell viability was assessed after 96 h in culture using a cell counting kit-8 (CCK-8) (Sigma Aldrich). Cells incubated in 0.1 % Triton-X (Sigma Aldrich) and L-15 were used as positive and negative controls, respectively. Blanks were also measured. Absorbance measurements at 450 nm were taken after 4 h of incubation at 20 °C using a Plate Reader Infinite® 200 PRO (TECAN).

2.7.3. Cell adhesion of embryonic fish cells on ULA wells with adipose ink coating showing defined surface condition

24-well ultra-low attachment (ULA) plates were coated with adipose inks covering the full bottom of the well and a thin coat around 5 mm of the well wall. To obtain a defined surface structure, a stamp was designed (Inventor) and 3D printed with PLA (Prusa) (Figs. S2b and c). After filling the well with the liquid ink at 80 °C, the stamp was pressed into the inks during gelation. The inks were submerged overnight in PBS with 5 % pen-strep.

PBS was removed and replaced by L-15 media 1 h prior to the seeding. Media was removed and a 25 μL drop with a high cell concentration (800,000 cells mL^{-1}) was added onto each sample and left for cell attachment for 60 min. Then, 500 μL of L15 were added and structures were incubated at 20 °C and media was changed every 2–3 d for 7 d. Wells without ink served as positive control.

Cell viability was assessed at day 7 using calcein-acetoxymethyl [0.2 %] solution in PBS (Sigma Aldrich #C1359) for viable cell-staining (green) and ethidium homodimer I (Sigma Aldrich, #E1903) for red-staining of dead cells [0.2 %] by fluorescence microscopy after 30 min of incubation with a Leica DMI3000B fluorescence microscope (Leica Microsystems) (n = 6). The images were merged and used to quantify viability using ImageJ software.

2.8. Texture profile analysis (double compression test)

For the texture profile analysis, a protocol from (Paredes, Cortizo-Lacalle, Imaz, Aldazabal, & Vila, 2022) was followed. Shortly, a double compression test (10 N load cell, compression machine from Univert) was performed with a preload of 0.01 N and a compression speed of 3 mm/s until a compression of 50 % was reached, and the movement was reversed. After a pause of 1 s the second cycle was performed equally to the first cycle. A schematic representation of the applied compression cycle can be seen in Fig. 2**a**. Casted structures of SFO40 and SFOwax inks were used for the assessment of the texture profile of pure fat structures. As food prototypes, firstly moulded samples were created, with 30 % fat-based ink (SFO40 or SFOwax) and a muscle-mimicking 1.5 % κ-CA ink coloured with 1 % red stain (Corante Encarnado frasco 28 mL, Globo) in MilliQ water. Therefore, 100 μL of the red ink was filled into the moulds (diameter of 9.5 mm and 10 mm in height), followed by 50 μL of fat-based ink. In total, three layers of each ink were added at 80 °C with a short pause between each layer to allow gelation. After 10 min at RT the moulds were carefully removed. Finally, 3D-structures were designed in Inventor (Autodesk, USA) consisting of alternating layers of 10 mm in diameter and 1 mm in height for the red stained ink, and 0.5 mm in height for the fat-based ink. In total, 4 layers were printed of each ink, reaching a height of 6 mm product using an Allevi 2 bioprinter (3D systems, USA). The settings for the three inks were the following: For the red-stained ink, a 25-gauge needle was used (0.25 mm inner diameter), and the printing was performed at around 9–10 psi with a constant temperature of 25 °C. The two different fat-based inks (SFOwax and SFO40) were printed with a 23-gauge needle (0.33 mm inner diameter) at 25 °C and 35 °C, respectively, with 9–10 psi and around 11–12 psi pressure. All samples were left in PBS overnight before measurements were performed (n = 5). For comparison, a fresh salmon fillet was obtained at a local supermarket, and cubes of around 15 x 15 × 15 mm^3 were cut and measured (n = 5). A 0.01 N threshold was used to reduce the background noise, and the following parameters were obtained from the graphs Fig. 2b using matlab (Version R2021a - MATLAB 9.10, MathWorks, US).

- The hardness is a measure for the stiffness of the product, and is equal to the maximal load F_1 in the first deformation cycle Fig. 2b
- The cohesiveness Co is a parameter for the consistency of the material and can be calculated using Equation (8) and the areas indicated in Fig. 2**b**:

$$\mathrm{Co}\,[-] = \frac{A_3 + A_4}{A_1 + A_2} \qquad \text{Eq. 8}$$

Values of Co = 1 indicate that the material does not get disintegrated during the first cycle, while values close to 0 indicate complete disintegration.

- The springiness Sp is an indicator for the recovery of the sample after the first compression and is related to its viscoelastic characteristics. It is calculated with the times t_1 and t_2 required to reach the maximum load in the first and second cycle, respectively, see Equation (9) Fig. 2b):

$$\mathrm{Sp}\,[-] = \frac{t_2}{t_1} \qquad \text{Eq. 9}$$

- The chewiness Ch combines the previously introduced parameters indicating how easily a product can be chewed, see Equation (10).

$$\mathrm{Ch}\,[\mathrm{N}] = F_1 * \mathrm{Co} * \mathrm{Sp} \qquad \text{Eq. 10}$$

- The resilience Re corresponds to the irreversible deformation of the material during the first cycle and can be calculated using the following Equation (11) Fig. 2**b**:

$$\mathrm{Re}\,[-] = \frac{A_1}{A_2} \qquad \text{Eq. 11}$$

If the material recovers entirely from the first compression (elastic deformation), Re = 1. With increasing plastic deformation, also the Re value increases.

2.9. 3D printing of prototypes

The printing process was performed using an in-house built 3D low-cost extrusion printer described elsewhere (Gusmão et al., 2022). This device consists of a modified 3D fused deposition modelling (FDM) low-cost 3D printer (Creality Ender-3 V2 3D printer, Creality, Shenzhen, China), which contains two temperature-controlled extruders [2 °C to

50 °C]. Two 3 mL syringe barrels (Nordson EFD Optimum, USA) with the corresponding pistons (Nordson EFD Optimum, Westlake, Ohio, USA) were filled up, and 23-gauge dispensing tips of 0.33 mm inner diameter were inserted. The 3D printed models consisted of a salmon sashimi-like prototype, as can be seen in Fig. 3a and a half shrimp-like prototype (Fig. 3b). These two models were designed in SolidWorks (Dassault Systèmes, France), and then sliced in a slicing software (Ultimaker Cura v5.0, Ultimaker B.V., Utrecht, Nederland). A red-coloured carrageenan-based ink was used to mimic the muscle part of the prototypes, containing 1.5 % κ-CA and 1 % red stain (Globo) in MilliQ water. The κ-CA was printed with a constant temperature of 22 °C and a velocity of 15 mm/s, and the deposition rate was set to 5 % on PronterFace (Pronterface https://www.pronterface.com/). The SFO40 ink was deposited with a constant temperature of 38 °C and a velocity of 30 mm/s, and the deposition rate was set to 8 % on PronterFace. For both inks, the layer height was set to 0.33 mm on Cura.

2.10. Statistics

Data is presented as mean values ± standard deviation. A Shapiro-Wilk test was used for assessing the normality distribution of the samples. Statistical differences were calculated using a one-way ANOVA (parametric data) and Kruskal-Wallis tests (non-parametric, $n < 5$). Statistical significance (*$p < 0.05$, **$p < 0.01$, ***$p < 0.001$, ****$p < 0.0001$) was evaluated by Post-hoc Dunn's multiple comparison tests for non-parametric data and Post-hoc Tukey pairwise comparison tests for parametric data using GraphPad Prism 7 (GraphPad, San Diego, CA, USA).

3. Results and discussion

3.1. Characterisation of fat-based formulations

Several optimisation steps were necessary to obtain fully vegan, printable inks with preparations based on previously reported 3D printable ink formulations of (Shi et al., 2021) (Beeswax, sunflower seed oil, whey protein powder, potato starch) and (Kamlow et al., 2021) (K-CA, T20, whey protein powder, sunflower oil). It was found that an oleogel with Carnaubawax at 5 % (w/w) gives the best printing results, while a higher Carnaubawax concentration of 10 % (w/w) led to very stiff oleogels that were hard to incorporate in the protein-polysaccharide formulation and impossible to print (preliminary results not shown). In their work, Shi et al. showed for beeswax-based formulations that an oleogel concentration of 20–30 % is optimal for printing, which was confirmed by our studies and the oleogel concentration was set to 20 % (w/w) to be able to obtain 3D printed constructs with fine shapes as a needle diameter of 0.5 mm or smaller was used for our printed models (preliminary results not shown). Contrary to Kamlow et al. we found an oil concentration of 40 % beneficial for the printing, as formulations with 10 % were too liquid for printing, and therefore the structures were bleeding and appeared almost transparent (preliminary results not shown).

In this study, the focus was placed on comparing different oil sources, namely SFO, RSO and OO directly and in combination with a vegan wax alternative, namely Carnaubawax. Only locally produced oil sources were considered for this work and selected due to their relevance in the European market (SFO and RSO), and more specifically OO was chosen due to its fundamental role in the Iberian, and Mediterranean cuisine (FEDIOL). Therefore, our approach consisted on developing six novel, fully vegan fat-based formulations: three emulsion inks containing 40 % SFO, RSO or OO (SFO40, RSO40 and OO40) and their three oleogel counterparts containing 20 % oil and Cwax (SFOwax, RSOwax and OOwax, respectively). For all six inks, the Young's modulus values were estimated from the linear region of stress-strain curves (Fig. S3). As reported in the literature, fat tissue shows non-linear dependency and the slope increases with the stress level, especially above 15–20 % strain (Comley & Fleck, 2010). There is a tendency for inks with 40 % oil to have higher values than the inks with 20 % oleogel, but no significant differences were found between the samples, with values ranging from 60 to 120 kPa (Fig. 4a). The fact that the oleogel-based inks were reaching similar Young's moduli as the oil-based inks with the double amount of oil can be linked to the presence of Cwax and its properties like hardness and melting point. Generally, natural waxes are blended with vegetable oils to increase the oil's hardness and viscosity at room temperature, e.g. in the formulation of lipsticks (Pan, Sivanathan, Kiepe, Kiepe, & Germann, 2021). Among them, Cwax possesses the highest hardness (17 N mm^{-2}) compared to palm oil (9 N mm^{-2}) and beeswax (2 N mm^{-2}), and a melting point of 82 °C–84 °C (Freitas et al., 2019; Sigma-Aldrich), giving it a brittle appearance at room temperature and leading to similar mechanical properties in our inks, compared to the formulations with oil only. All formulations show a comparable behaviour to a raw salmon fillet which is especially important for the development of sushi analogues where the fillet is not further processed and eaten in raw state. They are in the same order of magnitude to those reported for animal fat, for instance, Sun et al. reported that compression values for porcine adipose tissue are around 75 ± 40 kPa (Sun et al., 2021).

Important for the use in 3D printing of the food constructs, the time- and temperature-dependent behaviour was evaluated to find the gelation point of the formulations. As the storage modulus G′ is always above the loss modulus G″, the elastic properties of the fluid dominate (Hong et al., 2018). After 3 min, all materials were fully gelated at room temperature (RT) (Fig. S4). As it can be seen in Fig. 4b, the viscosity is lower in samples containing Cwax. For samples with 40 % oil the gelation point can be found at approximately 34 °C, and therefore around 2–4 °C higher compared to the samples with Cwax (30–32 °C).

For the use in food industry, not only the manufacturing and final high-quality product is important, but also the subsequent supply chain and according storage and delivery conditions. Therefore, the inks stability was evaluated under different storage conditions. Generally, both the polysaccharide and the protein used in our formulations are supporting the formation and stabilization of a long-term emulsion in neutral conditions. SPI leads to the formation of a stabilizing layer around the oil droplets at the oil–water interface due to its amphiphilic character as a protein and therefore acts as an emulsifier, and stabilizer (Dickinson, 2003; Tang, 2017). Indeed, in aqueous solutions, emulsions can already been formed by SPI alone (Gu, Campbell, & Euston, 2009; Xu, Yu, Xue, & Xue, 2023). However, K-CA as an edible polysaccharide stabilises the mixture by modifying the viscosity and influencing the thermoreversible gelation, leading to a more stable emulsion (S. Liu & Li, 2016; Xu et al., 2023).

To assess the stability of the inks, the weight loss was recorded during drying, being slightly higher than expected by the theoretical water content of the samples which is 78 % for samples with oil and Cwax and 58.2 % for samples with 40 % oil. The measured values consisted of 76.9 %, 76.3 % and 76,9 % for the samples with oleogel, and 69.2 %, 69.4 %, 66.6 % for the samples with 40 % oil, respectively (Fig. 4c). One possible explanation for the differences between the theoretical and the calculated values is the possible leakage of oil during the sample processing, affecting the final total weight. However, when submerged in phosphate buffer saline (PBS), the 40% oil samples seemed more stable (after 21 d: −7.8 %, - 8.7 %, and −7.7 % at RT and −10.0 %, −10.1 % and −6.0 % at 4 °C, respectively) than formulations containing Cwax. The low weight loss of OO40 samples is less implicit when considering the high standard deviation of this sample. At RT, samples containing Cwax lost around 20 % (after 21 d: −19.5 %, −18.7 % and −22.4 %) of their weight due to leakage of oil and dissolution, while at 4 °C, these oleogel-based inks showed higher stability (after 21 d: −13.8 %, −16.7 %, −13.1 %) (Fig. 4d). Thus, for future applications, storage conditions, like temperature, packaging conditions, and shelf life need to be considered to ensure the stability and quality of the final products.

The lower stability of the emulsion inks containing Cwax can also be observed in the cream index (Fig. 4e, Fig. S5). The higher the creaming index, the higher was the serum layer after the thaw-freeze cycles, indicating higher instability of the emulsion inks (Petrowski). Destabilized oil layers were observed in all samples, though the samples with Cwax showed larger serum layers and therefore higher creaming indices, of around 35–65 %. Samples with 40 % oil showed values around 10 % cream index, except for OO40 which also was less stable and showed values of 31.9 % ± 0.9 %. These results are supported by the findings of Wang et al. (Wang et al., 2023) In their studies, they examined the influence of different soybean oil concentrations to form emulsion gels using chitosan as polysaccharide and glycyrrhizic acid-zein composite nanoparticles as protein source. They found that gels with a volume fraction of below 30 % oil showed phase separation after a storage of 30 days. They explained this creaming instability with the increased oil droplet size and the insufficient number of droplets to form a stable 3D network, giving the droplets the chance to coalesce, move upwards and form a cream layer. In addition, the lower stability of the Cwax inks could possibly be related to the fact that in each thaw cycle, the melting point of the Cwax of around 83 °C was surpassed and the oleogels segregated (Freitas et al., 2019), stressing again the importance of storage temperature conditions.

Another explanation can be found in the droplet size and its distribution. Higher stability is linked with smaller droplet size (Petrowski), and overall, the droplets of samples with 40 % oil tend to show a smaller median size compared to the samples containing Cwax (Fig. 4f, Fig. S6). Also, when comparing the images of the samples with oleogel to the inks with 40 % oil, the latter show a more typical appearance of emulsion structure with oil droplets uniformly dispersed in the surrounding matrix, while the oleogel based inks possess larger areas with few droplets, which might be due to the lower fat concentration (Fig. 4g, Fig. S6). Wang et al. pointed out in their work the importance of sufficient lipid droplet formation to obtain droplet–droplet adhesion that allows the printability of the ink by forming a soft solid with adequate stability and mechanical properties (Wang et al., 2023). Though, between the samples only a significant difference ($p < 0.05$) was found between OOwax and RSO40 and between SFO40 and RSO40, mainly due to the large variation within the samples. The latter has the smallest range of values from 5.4 μm to 34.8 μm of all samples and generally the lowest median value compared to the other samples (23.7 μm, 29.1 μm, 27.3 μm for the inks with Cwax, and 29.0 μm, 15.7 μm and 23.3 μm for the inks with 40 % oil, respectively). In general, the droplet sizes fall within the range from 0.1 to 50 μm which is in accordance with normal food emulsion droplet sizes (Petrowski).

Finally, also the ζ-potential can be used as an indicator for emulsion stability. As shown before by Hong et al., the lower the particle size is, the smaller is the creaming index and the lower values are obtained as well in ζ-potential (Hong et al., 2018). In their paper, In Kwon Hong et al. measured zeta potentials of −40 to −30 mV, while creaming indices of that emulsion ranged from 35 to 75 %, respectively. Laying between −73 and −52 mV, all samples show negative values of ζ-potential (Fig. 4h). The trend of the values is thus supporting the results of the measured droplet sizes, and creaming indices. One exception is the high value of SFO40 (−52 mV), which does not match its low creaming index (10 %).

3.2. Characterisation of ink printability

The printability of the different formulations was then assessed by printing a one-layered mesh and up to 25-layered towers (Fig. 5a and Fig. 5b Fig. S7) using a nozzle diameter of 0.5 mm and extrusion pressures in a range of 4–20 psi regulated by the pneumatic dispensing unit. All inks showed good printability (Pr ≈ 1) with no significant differences between the samples (Fig. 5c). It was observed that the inks with Cwax tend to form rectangular pores with softer edges (Pr < 1), which can be observed especially for the sample with OOwax, while the inks with 40 % oil presented Pr values greater than 1, and therefore more cluttered pores.

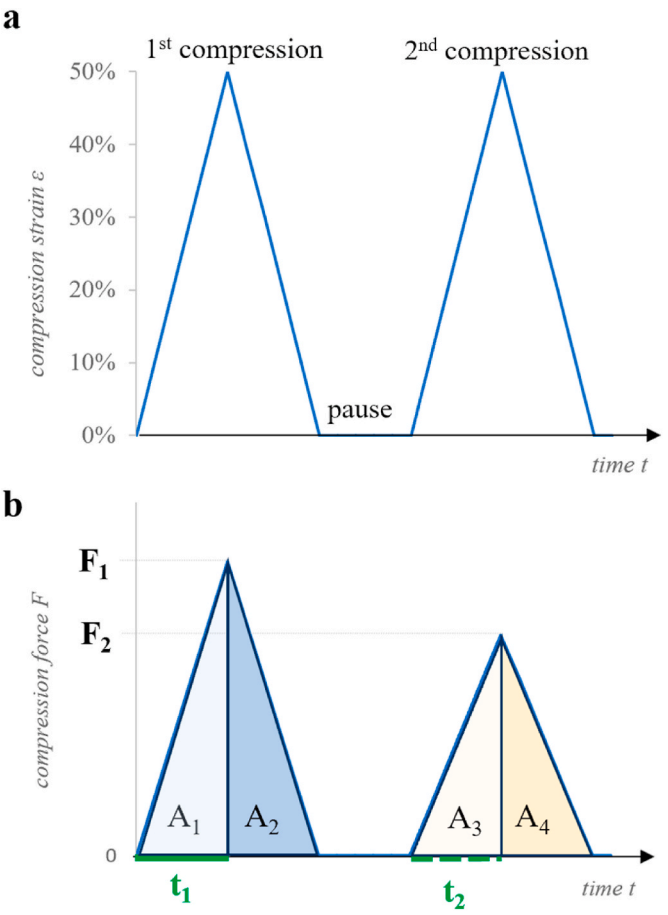

Fig. 2. (a) Scheme of the time-compression strain curve of the double compression test and (b) the obtained time-dependent compression force curve used to calculate the texture parameters like hardness, cohesiveness, springiness, chewiness and resilience.

To be able to print bigger constructs like an animal fillet, not only the shape fidelity of a single layer is important, but the quality and stability of multiple layers printed on top of each other. Therefore, round towers of 5, 10 and 25 layers were printed. Some differences were found in the structure's height after printing five layers (Fig. 5d). These differences decreased when more layers were printed, and no significant differences were found on the taller structures. All inks showed a linear dependency between the tower height and the number of layers printed, as expected, corresponding to a layer height of 0.445 ± 0.02 mm (R^2 = 97.6 %).

To be able to evaluate the product's shape fidelity for a longer time, printability values were assessed on printed meshes over a period of 2 weeks at different conditions. All inks presented constant Pr values when the printed structures were submerged in PBS due to the presence of ions stabilizing the κ-CA chains (Fig. 5e, Fig. S7) (Marques et al., 2022). An exception is the mesh printed with OO40, which was breaking apart after 1 d of incubation, making it impossible to take further measurements. Already in the characterisation of the adipose inks themselves, OO40 showed to be less stable, e.g. with higher creaming index. Without PBS, the structures lost water due to evaporation and leaked oil causing deformities on the structures that led to increased Pr-values due to more cluttered structures (Fig. 5f). However, this tendency was mainly found for samples with 40 % oil, where the structures occurred to be very unstable and running apart after 3d incubation in air while the samples with Cwax showed quite high accuracy and stable structures over the given time. Cwax works tentatively as preserving component, maybe

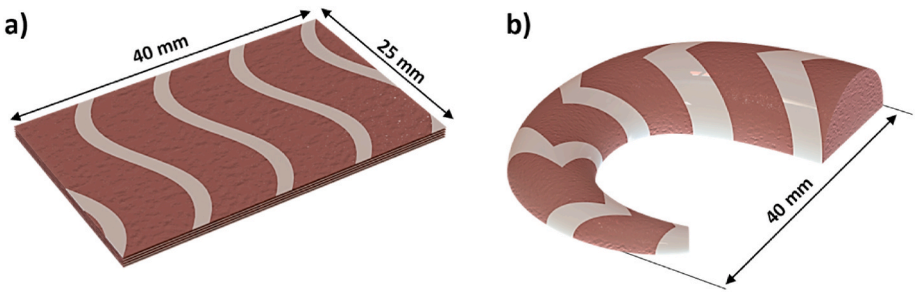

Fig. 3. Salmon sashimi-like (a) and half shrimp-like (b) CAD models.

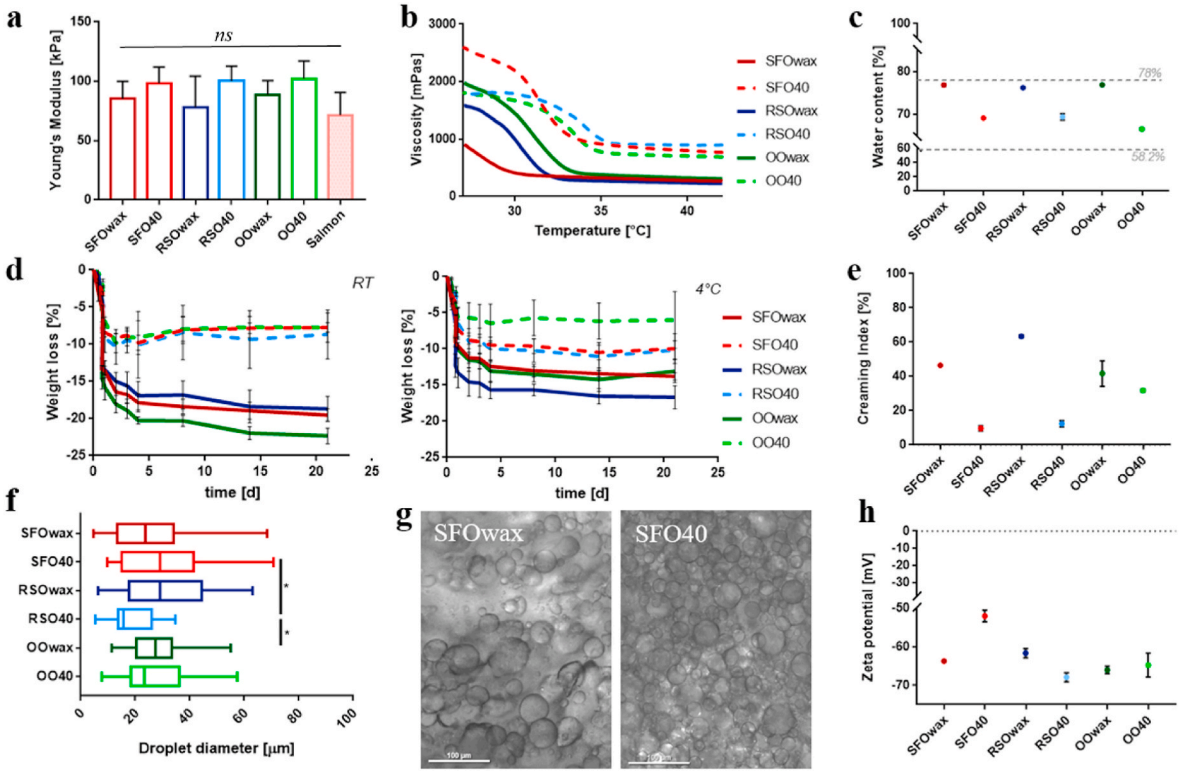

Fig. 4. Characterisation of fat-based formulations: (a) Young's Modulus obtained for stress levels between 20 and 40 %; Statistical significance (n = 5) was assessed with Tukey multiple pairwise comparison tests showing values with no significant difference. (b) Viscosity measurements show temperature dependence and gelation temperature of the samples (n = 3). (c) Water content obtained during drying at 40 °C for 5 d (n = 3). (d) Weight loss of samples taken during a time period of 21 d at room temperature (RT, left) and at 4 °C (right) (n = 3). (e) Cream index obtained after three freeze-thaw cycles (n = 3). (f) Droplet diameter. Statistical significance (n = 30) was assessed with Dunn's multiple comparison tests showing values with significances (*p < 0.05). (g) Exemplary microscopy images (20x) of SFOwax and SFO40 displaying their microscopic structure taken from printed mesh structures (h) Zeta potential obtained for the different emulsion inks with values between −50 and −70 mV (n = 3). Data shown indicate mean ± 1SD.

due to its anti-oxidant and barrier properties, stabilizing the structures when exposed to air (Freitas et al., 2019). Overall, it was possible to conclude that it is possible to print multi-layer structures with high shape fidelity with the three different oils and oleogels. As shown during the stability measurements in air or PBS, storage medium is important, as liquids are tending to dissolve samples with Cwax, while under air-condition, the Cwax is stabilizing the structures, emphasising again the importance of storage conditions.

3.3. Formulation of enriched inks using omega-3 (ω-3) oil

After the preliminary characterisation of the different formulations, SFO-containing inks were selected for their enrichment with omega-3 (ω-3) oil. Inks with RSO were excluded due to their cytotoxic performance according to EN ISO 10993-5 (International Organization for Standardization, 2009) (viability <40 %, Fig. S8), while inks containing OO were discarded due to their low stability, and less pleasant, greenish colour. ω-3 oil is one of the most important nutrients contained in fish meat. In sea bass fillets, approximately 35 % of the fatty acids are polyunsaturated fatty acids (PUFAs), which makes this fish an important source of essential ω-3 fatty acids, like docosahexaenoic acid (DHA) and eicosapentaenoic acid (EPA) that are not or are only slowly synthesized in humans (Kocatepe & Turan, 2012; Periago et al., 2005; The Good Food Institute Asia Pacific 2022). As SFO itself does not naturally contain essential ω-3 PUFAs (The Good Food Institute Asia Pacific 2022), 5 % of the SFO was replaced by two types of ω-3 oil extracted from algae to improve the nutritional value of the newly developed inks.

The first source of ω-3 oil had to be extracted from carrageenan-based capsules. It contained a higher concentration of ω-3 fatty acids from seaweed oil (containing EPA at 25,000 mg 100 mL^{-1} and DHA at 41,667 mg 100 mL^{-1}) and included also high oleic sunflower oil, rosemary extract, tocopherols (vitamin E), and ascorbyl palmitate (fat-

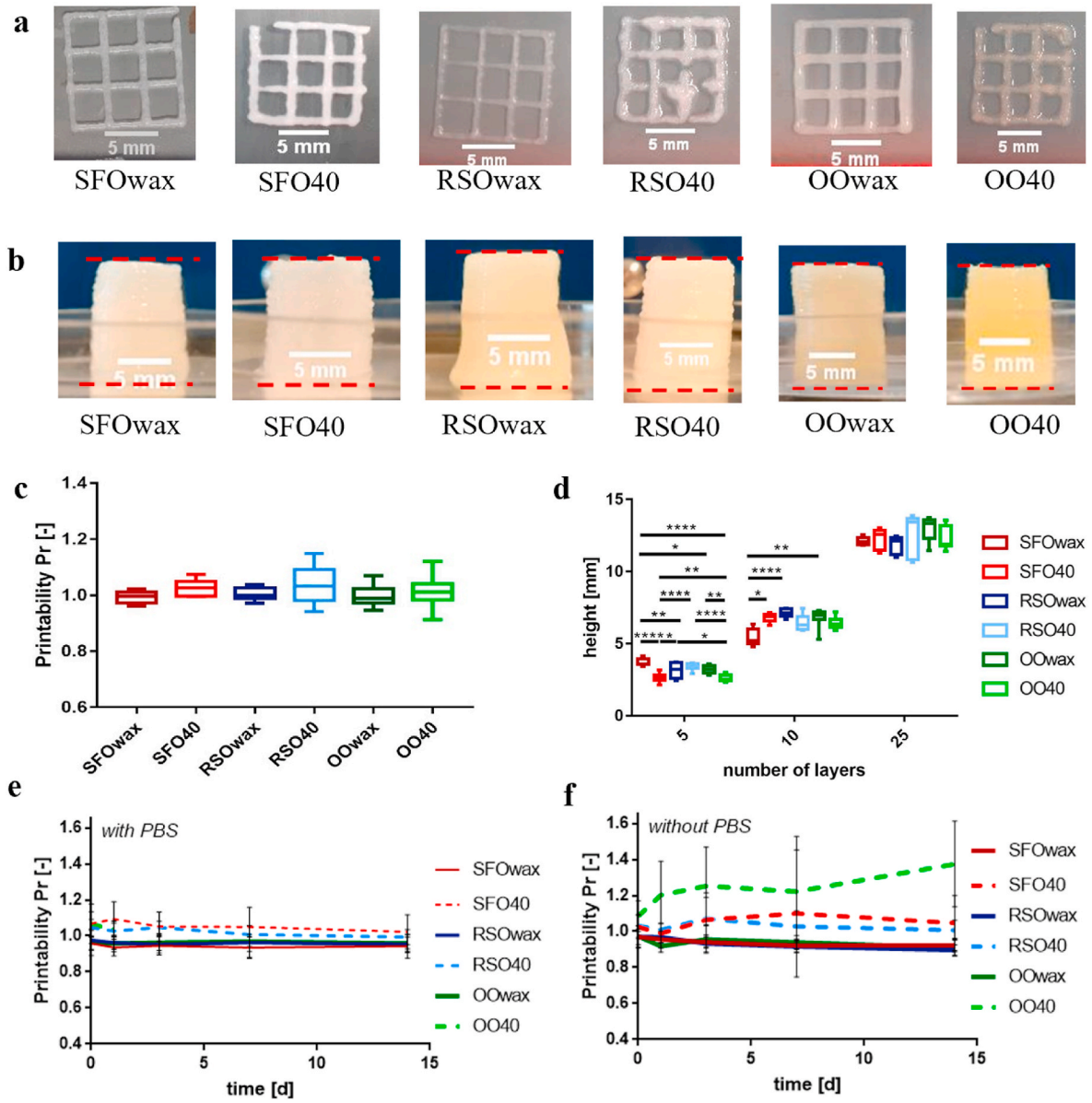

Fig. 5. Printing results of the six different inks showing meshes with nine pores (a) and towers of 25 layers height (b). Characterization of ink printability (c) showing printability value. No statistical significance (n = 9) was found using Kruskal Wallis significance testing ($p > 0.05$). (d) Height increased with increasing number of layers showing equal slopes of 0.445 mm and intercept of 1.39 mm ($R^2 = 97.6$ %) obtained with linear regression analysis (n = 9). Statistical significance was found with different significance values (*$p < 0.05$, **$p < 0.01$, ***$p < 0.001$, ****$p < 0.0001$) evaluated by Tukey pairwise comparison tests for parametric data (number of layers = 5) and Dunn's multiple comparison tests for non-parametric data (number of layers = 10). No statistical difference was found for the samples with 25 layers (non-parametric, $p > 0.05$). Printability development over 2 weeks of meshes submerged in PBS (e) and without PBS (f) (n = 10–15). Data shown indicate mean ± 1SD.

soluble vitamin C), thus, providing a vegan ω-3 rich oil. The second source comprised less concentrated seaweed oil, (containing DHA at 4000 mg 100 mL^{-1}), medium chain triglycerides of coconut and cholecalciferol (vitamin D3 at 2000 μg 100 mL^{-1}). Inhibiting higher potency than plant-based vitamin D2, cholecalciferol is the main vitamin D supplement mostly sourced from lanolin that is naturally contained in sheep's wool grease (Hirsch, 2011; Schmid & Walther, 2013). Therefore, it is limiting its use in fully plant-based formulations (PubChem, 2022a). However, as sustainable developments in the food industry also include the exploitation of non-vegan by-products as yet unused sources of nutritious food (e.g. seafood waste (Suresh, Kudre, & Johny, 2018)), it was also included for comparison.

Regarding the compression values, when 5 % of the SFO was replaced by ω-3 rich oil, the compression values were significantly increased in comparison to salmon (71.25 kPa) and SFO-based (85.49 kPa for SFOwax and 98.01 kPa for SFO40) formulations without ω-3 rich oil, reaching values of Young's Modulus between 110 and 180 kPa (Fig. 6a, Fig. S9). As one possible reason for the different behaviour in mechanical tests we suggest some stearic alternation due to the rather linear vitamin molecules or stearic hindrance due to the huge 3D ω-3 molecules (PubChem, 2022b; 2022c). SFO itself consists mainly of triglycerides composed by unsaturated fatty acids (14–34 % of $C_{18:1}$ and 55–73 % of $C_{18:2}$) with some 8–15 % (5.5–8 % of C_{16} and 2.5–6.5 % of C_{18}) saturated fatty acids (Thomas).

However, the rheological behaviour is very similar to the SFO40 and SFOwax inks, as the inks with ω-3 show gelation points at approximately 32 °C for inks containing 40 % oil and 30 °C for oleogel-based inks, respectively (Fig. 6b, Fig. S10), Also the droplet diameters are

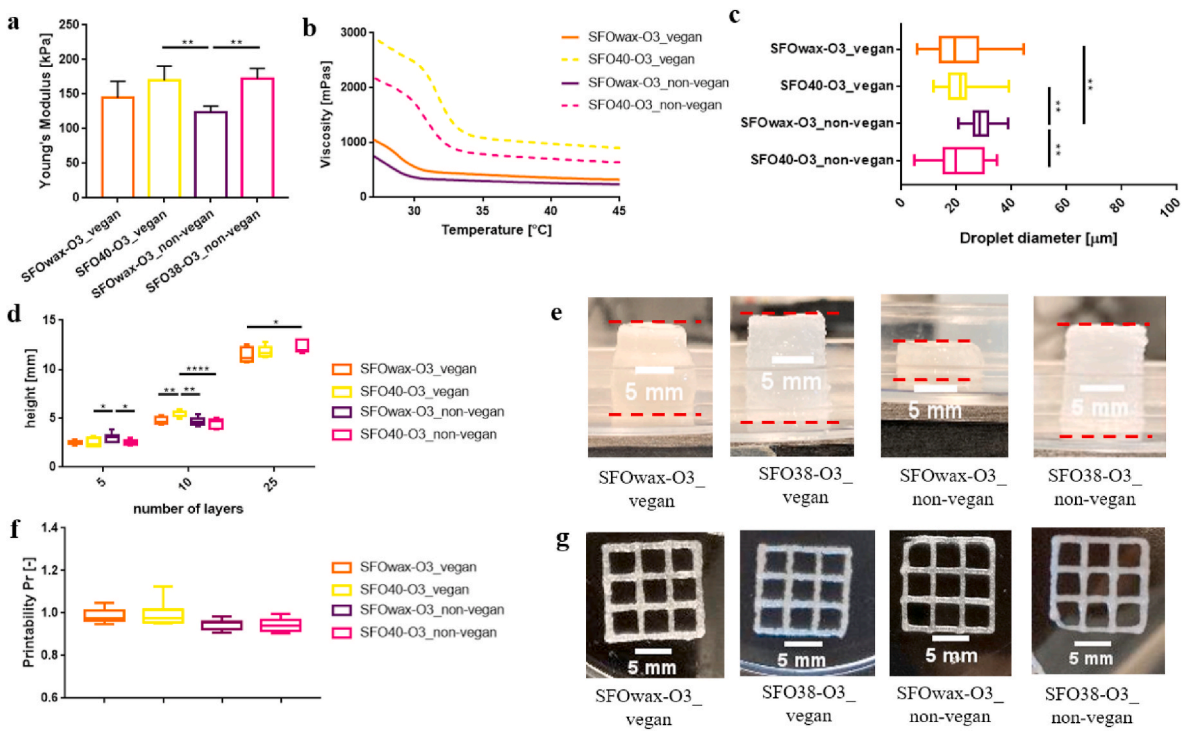

Fig. 6. Characterisation of ω-3 enriched inks: (a) Young's Modulus obtained for stress levels between 20 and 40 %; Statistical significance (n = 5) was assessed with Tukey multiple pairwise comparison tests showing values with significance (**p < 0.01). (b) Viscosity measurements show temperature dependence and gelation temperature of the samples (n = 3). (c) Droplet diameter. Statistical significance (n = 30) was assessed with Dunn's multiple comparison tests showing values with significances (**p < 0.01). (d) Height increase with increasing number of layers showing equal slopes of 0.454 mm and intercept of 0.647 mm (R^2 = 99.2 %) obtained with linear regression analysis (n = 9). Statistical significance was found with different significance values (*p < 0.05, **p < 0.01, ***p < 0.001, ****p < 0.0001) evaluated by Dunn's multiple comparison tests for non-parametric data (number of layers = 5) and Tukey pairwise comparison tests for parametric data (number of layers = 10). No statistical difference was found for the samples with 25 layers (non-parametric, p > 0.05). (e) Printing results of the different inks containing ω-3 showing towers of 25 layers height. (f)) Characterization of ink printability showing printability values measured on printed meshes (n = 1) with nine pores (g). Statistical significance (n = 9) was assessed with Dunn's multiple comparison tests showing values with no significance (p > 0.05).

comparable to previously obtained values for SFOwax and SFO40 inks and span around 5–45 µm (Fig. 6c, Fig. S11). Only the sample of SFOwax-O3_non-vegan showed significant difference compared to the three other inks containing ω-3. This ink has the lowest range of values in this group (20–38 µm) with the highest median of 28 µm which might explain the measured difference. As indicated before, bigger droplet diameter led to less stable emulsion which was also noticed during printing, as SFOwax-O3_non-vegan ink was difficult to print and towers of 25 layers collapsed after printing (Fig. 6d and e). Generally, very accurate (R^2 = 99.2 %) linear dependency was found between the number of layers printed, and the tower height, which can be expressed by a slope of 0.454 mm and intercept of 0.647 mm (Fig. 6d). The printability of all four ω-3 containing inks is very close to 1 without any significant difference (Fig. 6f and Fig. 6g).

3.4. Biocompatibility assessment

The influence and interaction of the inks with DLEC (*Dicentrarchus labrax* Embryonic Cell Line) cells were evaluated to assess their cytocompatibility and potential applications in the manufacturing of cell-based seafood products. Firstly, a leakage assay was performed where media incubated together with the various inks was used for cell growth. The viability results were assessed using a cell counting kit-8 (CCK-8) as can be seen in Fig. 7a. Inks with Cwax tend to lead to lower viability (53–62 %) compared to the inks without Cwax (71–81 %), approving the non-cytotoxicity of the latter. Higher leakage of material into the media could be one reason for the lower viability in inks with Cwax, as it was observed during the stability studies performed over a 3-week period (Fig. 4d).

In the second assay, direct contact between the inks and DLEC cells were studied. Therefore, moulded samples were placed on top of a confluent cell layer and the cell density was assessed after 7 d of culture using Trypan blue staining. Similar tendencies were found (Fig. 7b), however, results for SFOwax and SFOwax-O3_vegan are considerably low, where the cells only roughly doubled with 47,000 and 32,500 counted cells compared to 20,000 seeded cells, reaching only 36 % and 25 % of the cell count in the control well (130,000 cells). All inks containing 40 % oil show higher cell count compared to the inks with Cwax, with the ink SFO40 standing out positively with almost five times as much cells as seeded reaching a cell count of 97,500 cells after 7 d of culture (75 % of positive control). No visual examination of the wells was possible while the samples were in place due to their opacity and the applied plastic structure on top of the scaffolds, which guaranteed direct contact between the inks and the cells. Thus, it might be difficult to conclude whether cell death occurred due to the oil leakage to the culture media or just by direct contact with the material. Another possibility is the lack of nutrients and oxygen diffusion to the cells due to the physical presence of the inks being pressed on the cell layer. In future, the moulded scaffolds could be increased in height, and the shape could be changed from cylindrical to a truncated cone structure, so that only a slight pressure is exhibited directly from the cover slip onto the scaffold, keeping them in place without the need to apply a plastic structure, thus making it possible to observe the contact area between the scaffolds and the cell layer during the experiment.

In the final adhesion assay, DLEC fish cells were seeded in high concentration (800,000 cells mL^{-1}) onto inks with a defined, structured surface, to trap them onto the scaffolds, thus allowing the evaluation of the cell adherence to the scaffolds (Figs. S2b and S2c). In all scaffolds,

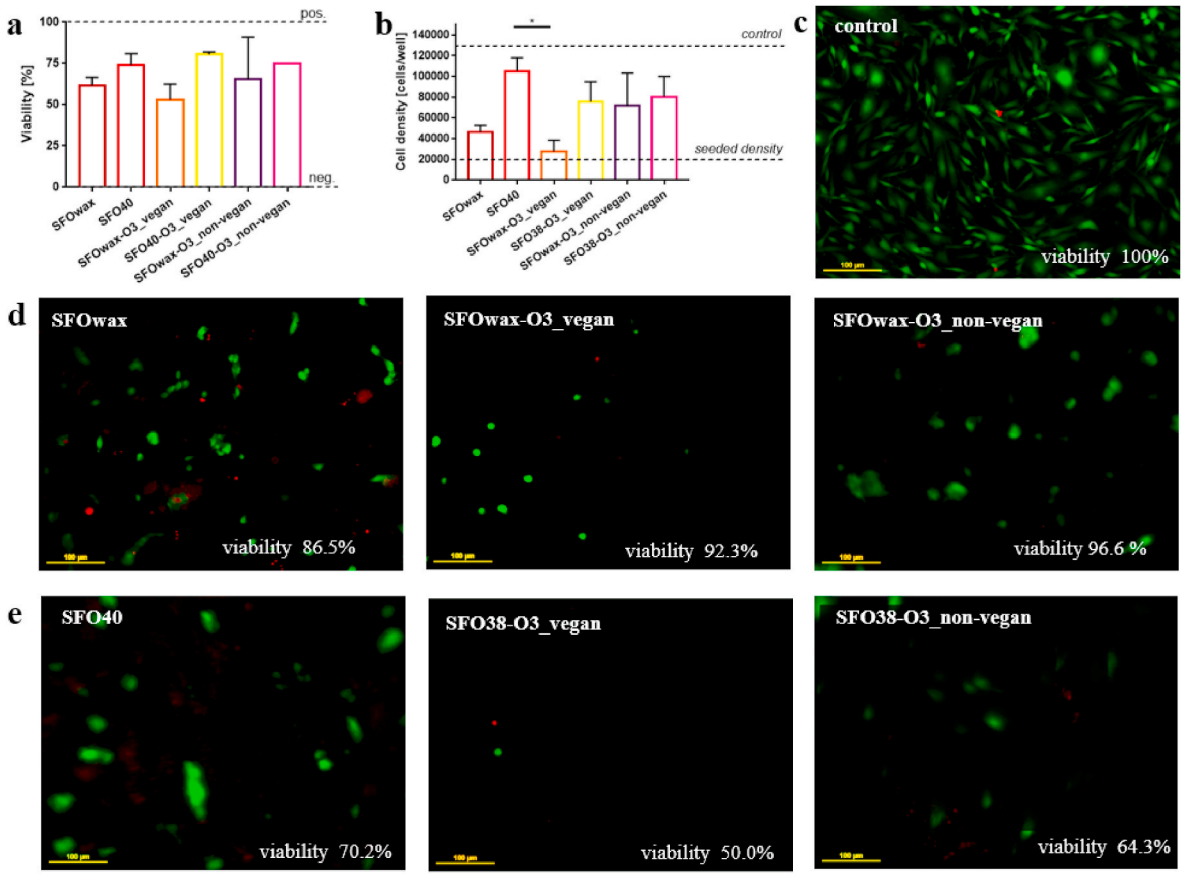

Fig. 7. Characterization of ink biocompatibility (a) showing viability values of the CCK-8 viability assay with media change, including positive and negative control. No statistical significance (n = 3) was found using Kruskal Wallis significance testing ($p > 0.05$). (b) Cell density after 7 d of incubation with casted samples placed on top of confluent plates compared to a control plate without ink and the seeded initial density (n = 3). Statistical significance was found (*$p < 0.05$) evaluated by Dunn's multiple comparison tests for non-parametric data. Images (c) to (i) show fluorescence images of live-dead stained cells of the adhesion assay with (c) being the control plate, (d) showing the oleogel-based inks (SFOwax, SFOwax-O3_vegan, and SFOwax-O3_non-vegan), and (e) the inks with 40 % oil (SFO40, SFO38-–O3_vegan, and SFO38–O3_non-vegan). Data shown indicate mean ± 1SD.

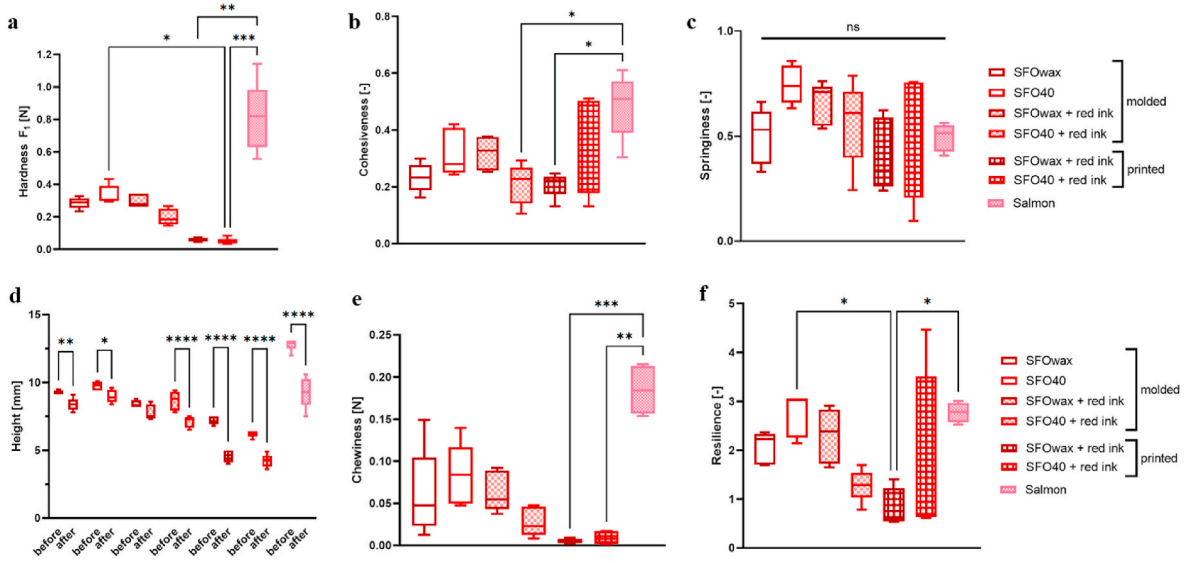

Fig. 8. Characterization of sensory properties obtained from a double compression test. (a) Hardness, (b) Cohesiveness, (c) Springiness, (d) height change from before to after the double compression, (e) Chewiness, (f) Resilience. All tests were performed on moulded samples of pure SFOwax ink and SFO40 ink, moulded samples of SFOwax and SFO40 combined with a red-stained k-CA ink, respectively, and printed samples of SFOwax and SFO40 inks combined with red-stained k-CA ink, respectively. For comparison, also a fresh Salmon fillet was included. Statistical significance (n = 5) was assessed with Dunn's multiple pairwise comparison tests showing values with different significances (*$p < 0.05$; **$p < 0.01$, ***$p < 0.001$, ****$p < 0.0001$).

lower cell number was found and more round morphology of the cells compared to the control plate with the typical elongated shape of cells attached to plastic surface (Fig. 7c). Contrary to the results obtained in the previous assays, higher cell viability of 86.5 %–96.6 % was found in inks with Cwax. As can be seen in Fig. 7d, these inks also show higher cell numbers compared to the inks with 40 % oil (Fig. 7e) Besides the influence of the Cwax, also the lower fat content of only 20 % compared to 40 % oil in the other inks could be beneficial in providing more space for the cells to attach due to the hydrophilic surrounding.

However, while the structured surface with the grooves and holes helped to trap the cells and supported their attachment, the uneven surface made it more difficult to achieve a good visualisation of the cells by fluorescence microscopy as it was not possible to focus all the cells on the same plane as in the control. There also seemed to occur a certain interaction between the live/dead probes used in this assay and the inks as some artifacts could be observed, where wax and/or oil bubbles were fluorescent with both red and green filter (Fig. S12). However, as the areas where artifacts occurred were very minor, and clearly distinguishable from cells due to their yellow colour, they did not affect the acquisition of the images.

3.5. Texture analysis

For applications in cultured meat, and especially to reach customer acceptance, it is crucial for the developed cell-based product to mimic the sensory properties of their traditional meat counterparts. Therefore, the six indicators presented in Fig. 8 were obtained in a double-compression test with a compression of 50 % (Figs. S13 and S14). Compared to a fresh salmon fillet (0.81 N), the developed inks SFOwax and SFO40 inherit a lower stiffness, however not significant (Fig. 8a). As the Young's Modulus of 1.5 % k-CA ink is similar to the developed fat-based ink (~80 kPa), the hardness of the moulded hybrid samples is very similar to the moulded pure samples (0.29 N vs. 0.30 N for SFOwax, respectively and 0.34 N vs. 0.2 N) (Marques et al., 2022). However, the hardness decreases when these inks are printed in combination with the red-coloured ink, reaching a significant lower value compared to salmon fillet (0.06 N and 0.05 N for SFOwax and SFO40 printed, respectively). The decrease in hardness could be explained by the manufacturing process as such, as for the printed samples, the layers were clearly separated, while during the moulding process marbled structures were obtained (Figs. S15b and S15c). In their work, Shahbazi et al., 2021 used different polysaccharides (starch, cellulose, inulin) at 2.5–6.7 % to stabilize their emulsion formulations. Their printed structures obtained higher hardness values (10–16 N), however, their inks contained only 10 % canola oil, and a much higher content of SPI (40 wt-%), trying to reach values of commercial meat analogues of 19.6 N. Yet, very little comparative studies on purely fat-based inks were performed so far in literature (Hu, Zhou, & McClements, 2022) and values for combined products are mainly obtained on unstructured samples (Samard & Ryu, 2019; Yen et al., 2023). Particularly, values for fish fillet-mimicking structures are lacking and although there are various studies on sensory properties of fish fillets, they are mainly performed on cooked samples rather than raw fillets (Farmer, McConnell, & Kilpatrick, 2000; Lazo et al., 2017). Finally, it has to be considered that there are variations in sensory properties between and within fish species, e.g., regarding their age, size, fat content, nutrition and postmortem treatment. Also, within one fish fillet the texture is not uniform, due to segmentation, and orientation (Hyldig and Nielsen, 2001; Lazo et al., 2017). As the middle section of a fish fillet showed to be most representative for the whole sample, the raw salmon samples were taken also from this part of this fish (Hyldig and Nielsen, 2001).

In Fig. 8b, the cohesiveness of the different samples is shown. Generally, the values indicate that all the samples are prone to disintegration, as they are closer to 0 than to 1, which can also be seen in Fig. S15 showing representative images of the samples before and after double-compression. However, also the values for the salmon fillet range from 0.3 to 0.6, while it is deformed reversibly without disintegration (Fig. S15d). Similar values for cohesiveness are also found for raw cultured-meat and real burger patties (0.24–0.56) (Yen et al., 2023), as well as for non-processed raw breast chicken fillet (0.3–0.7) (Paredes et al., 2022). The values for the moulded samples range between 0.1 and 0.42, and for the printed from 0.07 to 0.49, showing a wide range especially for the SFO40 + red ink - printed sample. This can be attributed to the low forces measured and the therefore more significant background noise found in these samples (Figs. S14e and S14f).

Due to this variability, there is also a high range in values for the springiness in the printed samples (Fig. 8c). Generally, the recovery in the SFO40 sample was the greatest (75 %), and the SFOwax sample (50 %) reached the closest to the salmon fillet (49 %), without any significant difference being found between all the samples. These results in springiness are supported by the measurement of the samples height before and after the test, showing a significant decrease in all samples except the moulded SFOwax + red ink samples (Fig. 8d, Fig. S15b). The chewiness is obtained combining the results of hardness, cohesiveness and springiness in one value indicating how easy the sample can be bitten (Fig. 8e). It becomes clear once more that printed constructs achieve significantly lower values (0.0051 N and 0.006 N for SFOwax and SFO40-printed with red ink, respectively) compared to the raw salmon fillet (0.18 N), which could be due to the fibrous, high-protein tissue being stiffer, and less prone to disintegration compared to the developed structures. Finally, Fig. 8f shows the resilience of the materials, indicating their plastic deformation with values greater 1 for most of the samples (Fig. S15). The high variation in the values for the printed samples, can be again attributed to the low forces measured.

The results of the sensory properties underline the increased difficulty to create a structured cell-based product, in regard to the more time-cosuming 3D printing processes compared to simple mixing and moulding for unstructured food. The sensory properties are also greatly influenced by the manufacturing method, making it harder to obtain a similar hardness, cohesiveness but also chewiness compared to traditional whole muscle-type meat. However, as a fish fillet is made up of 2–5 % fat tissue only, the main contribution to the sensory properties will be given by the protein-based muscle component, that was rather poorly replaced by the basic red-coloured k-CA ink (Kazir & Livney, 2021).

3.6. Manufacturing of prototypes by 3D printing

To demonstrate the further applicability of the fat-based inks developed in this work, complex 3D prototypes were designed and printed using an in-house built 3D extrusion-based bioprinting system. For this, the SFO40 ink, which showed promising results in mechanical properties, stability, and printing behaviour as well as viability and cell density, was selected.

Two different prototypes were developed: a sashimi-like fish fillet and a shrimp, using a plain k-CA ink containing red food colouring mimicking the muscular part of the structures and the SFO40 ink to create the fat tissues. In both cases, the final construct was very robust and the different materials were well integrated, allowing for their manipulation after printing using a spatula and tweezers (Fig. 9). This is essential for their food applications as materials will be subjected to mechanical stress during their manipulation for preparation and consumption. There have been developments of fat based inks that are printable in complex multi-layer constructs (Tian et al., 2021; Wen, Che, Kim, & Park, 2021), however, the stable printing of multi-material constructs combining a vegan fat-based ink with a second food-grade ink in the form of complex food prototypes with a printing height of up to 10 mm is unprecedented in the 3D printing of food structures.

Overall, it is possible to conclude that SFO40 is compatible with the 3D printing process for the development of more complex structures not only for cellular agriculture applications but also for the 3D printing of plant-based food products.

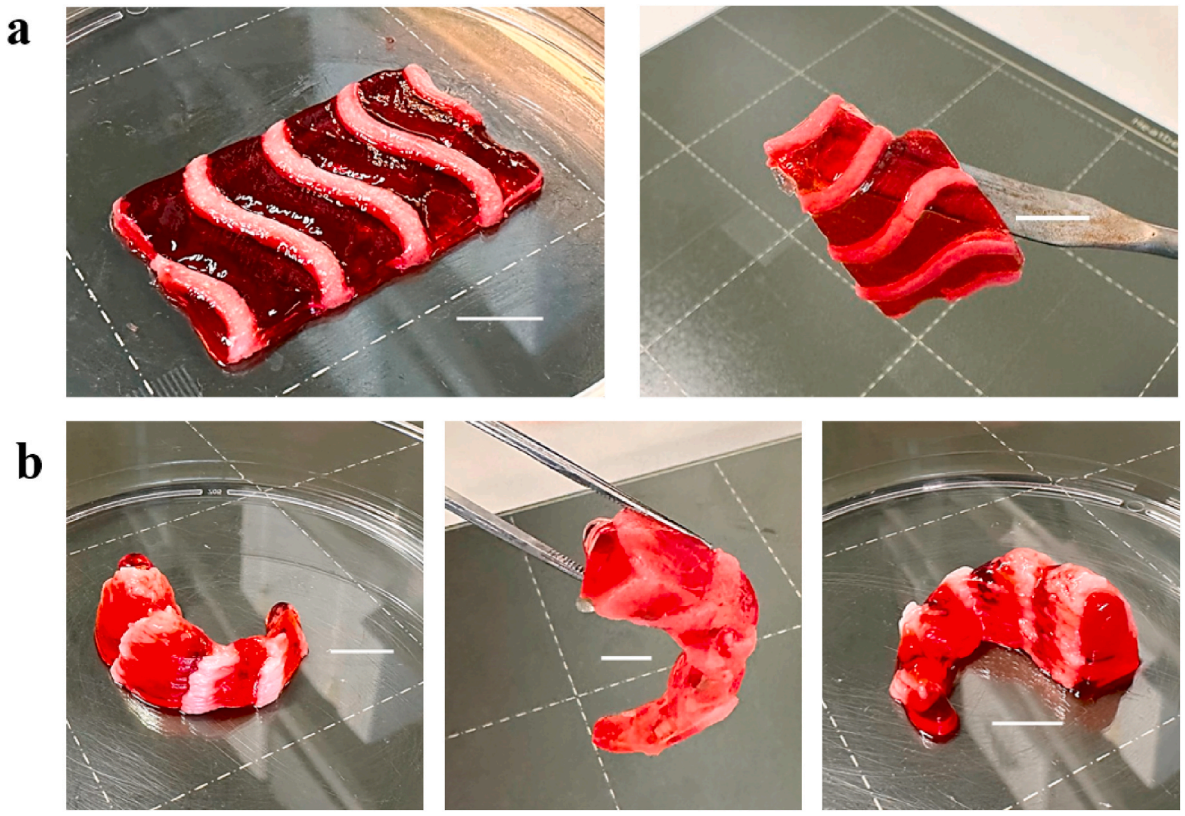

Fig. 9. Development of complex 3D printed seafood-like prototypes consisting on (a) a sashimi-like fish fillet and (b) a shrimp. Designs consist on a plain κ-CA ink with red food colouring mimicking muscle tissues and SFO40 as adipose tissues. Scale bars = 10 mm.

4. Conclusion

In this study, fully vegan printable fat-based inks were developed containing SFO, RSO and OO with potential applications in the development of cell-based seafood products for the first time. Mechanical behaviour was comparable with animal adipose tissue and printing properties allowed for the manufacturing of complex and structured edible prototypes of a sashimi-like fish fillet and a shrimp.

We concluded that the best fat-based inks corresponded to SFOwax and SFO40 due to their printability, natural fat colour, and promising results in viability studies. The nutritional value of the inks was also tuned by enrichment with plant-based omega-3 which are essential fatty acids that are naturally contained in fish and important for a balanced diet.

Some significant differences were found in the different ink's properties like multi-layer printability and shape fidelity, their compression modulus as well as in their biocompatibility which might require further investigation. For instance, inks enriched with omega-3 showed increased compression modulus compared to animal tissue, however, the right texture is a key feature for consumer acceptance of fish meat alternatives. Furthermore, structures with more than 10 layers were not possible to be printed with SFOwax-O3_non-vegan ink, which makes challenging its application in the 3D printing of complex structures. For the application in cellular agriculture food products, biocompatibility and sensory properties are crucial. The cell adherence of DLEC fish cells showed to be promising with SFO40 based inks, with acceptable cell viability, which are important findings regarding their final use with fish cells and other muscle-like materials in a whole-cut meat product. The texture analysis showed promising results, which will be further analysed in a future product containing also a protein-based muscle-like ink.

In the future, it would also be of interest to evaluate their compatibility and printing/bioprinting with other cell types such as chicken, bovine and porcine cells to investigate their applications in other cellular agriculture products. The evaluation in combination with materials exhibiting a high protein content as replacement for muscle tissue, as well as combining the fat inks with materials enriched in nutraceuticals and flavours to investigate the contribution of the fat-based inks to the organoleptic properties will contribute to a more holistic picture in terms of the final application in a vegan sustainable meat analogue.

Funding

The Good Food Institute (GFI) supported this work with its competitive Grant Program through the "Algae2Fish" project. This work was financed by national funds from FCT—Fundação para a Ciência e Tecnologia, I. P., through funding of CleanFish project (2022.07677), the PhD scholarship (2022.12900.BD, 2023.00599.BD), iBB-Institute for Bioengineering and Biosciences (UIDB/04565/2020 and UIDP/04565/2020), i4HB—Associate Laboratory Institute for Health and Bioeconomy (LA/P/0140/2020), CQE—Centro de Química Estrutural (UIDB/00100/2020) and IDMEC through LAETA project (UIDB/50022/2020). The work developped is on the scope of FEASTS (Project ID 101136749) funded by the European Commission funded in the call HORIZON-CL6-2023-FARM2FORK-01-13. Funding from Doctoral INPhINIT Incoming fellowships 2023 BECA reference LCF/BQ/D123/11990049 is acknowledged.

Institutional review Board Statement

Not appliable.

Informed Consent Statement

Not appliable.

CRediT authorship contribution statement

Kristin Schüler: Writing – original draft, Investigation, Conceptualization. **Diana M.C. Marques:** Writing – review & editing, Investigation. **Afonso Gusmão:** Writing – review & editing, Investigation. **Madalena Jabouille:** Investigation. **Marco Leite:** Supervision. **Joaquim M.S. Cabral:** Writing – review & editing, Funding acquisition. **Paola Sanjuan-Alberte:** Writing – review & editing, Supervision, Funding acquisition, Conceptualization. **Frederico Castelo Ferreira:** Writing – review & editing, Supervision, Funding acquisition, Conceptualization.

Declaration of competing interest

The authors declare that they have no known competing financial interests or personal relationships that could have appeared to influence the work reported in this paper.

Data availability

Data will be made available on request.

Acknowledgments

Prof Ana Paula Serro is acknowledged for providing access to the rheometer used in this work. “la Caixa” Foundation is acknowledged for the Postdoctoral Junior Leader Fellowship granted to P.S.-A.

Appendix A. Supplementary data

Supplementary data to this article can be found online at https://doi.org/10.1016/j.foodhyd.2024.110369.

References

Buonocore, F., Libertini, A., Prugnoli, D., Mazzini, M., & Scapigliati, G. (2006). Production and characterization of a continuous embryonic cell line from sea bass (Dicentrarchus labrax L.). *Marine Biotechnology, 8*(1), 80–85. https://doi.org/10.1007/s10126-005-5032-2

Comley, K., & Fleck, N. A. (2010). A micromechanical model for the Young’s modulus of adipose tissue. *International Journal of Solids and Structures, 47*(21), 2982–2990. https://doi.org/10.1016/j.ijsolstr.2010.07.001

Dekkers, B. L., Boom, R. M., & van der Goot, A. J. (2018). Structuring processes for meat analogues. *Trends in Food Science & Technology, 81*, 25–36. https://doi.org/10.1016/j.tifs.2018.08.011

Dickinson, E. (2003). Hydrocolloids at interfaces and the influence on the properties of dispersed systems. *Food Hydrocolloids, 17*(1), 25–39. https://doi.org/10.1016/S0268-005X(01)00120-5

Fahmy, A. R., Amann, L. S., Dunkel, A., Frank, O., Dawid, C., Hofmann, T., … Jekle, M. (2021). Sensory design in food 3D printing – structuring, texture modulation, taste localization, and thermal stabilization. *Innovative Food Science & Emerging Technologies, 72*, Article 102743. https://doi.org/10.1016/j.ifset.2021.102743

Farmer, L. J., McConnell, J. M., & Kilpatrick, D. J. (2000). Sensory characteristics of farmed and wild Atlantic salmon. *Aquaculture, 187*(1–2), 105–125. https://doi.org/10.1016/S0044-8486(99)00393-2

FEDIOL. EU vegetable oil and proteinmeal industry in the supply chain: - the EU vegetable oil and proteinmeal industry association. Retrieved from https://www.fediol.eu/data/Fediol_Brochure_A5_20_FINAL_.pdf.

Freitas, C. A. S. de, Sousa, P. H. M. de, Soares, D. J., Da Silva, J. Y. G., Benjamin, S. R., & Guedes, M. I. F. (2019). Carnauba wax uses in food - a review. *Food Chemistry, 291*, 38–48. https://doi.org/10.1016/j.foodchem.2019.03.133

Grossi, G., Goglio, P., Vitali, A., & Williams, A. G. (2019). Livestock and climate change: Impact of livestock on climate and mitigation strategies. *Animal Frontiers: The Review Magazine of Animal Agriculture, 9*(1), 69–76. https://doi.org/10.1093/af/vfy034

Gu, X., Campbell, L. J., & Euston, S. R. (2009). Effects of different oils on the properties of soy protein isolate emulsions and gels. *Food Research International, 42*(8), 925–932. https://doi.org/10.1016/j.foodres.2009.04.015

Guo, J., Gu, X., & Meng, Z. (2024). Customized 3D printing to build plant-based meats: Spirulina platensis protein-based Pickering emulsion gels as fat analogs. *Innovative Food Science & Emerging Technologies, 94*, Article 103679. https://doi.org/10.1016/j.ifset.2024.103679

Gusmão, A., Sanjuan-Alberte, P., Ferreira, F. C., & Leite, M. (2022). Design, fabrication, and testing of a low-cost extrusion based 3D bioprinter for thermo-sensitive and light sensitive hydrogels. *Materials Today: Proceedings, 70*, 148–154. https://doi.org/10.1016/j.matpr.2022.09.010

Hirsch, A. L. (2011). Industrial Aspects of vitamin D. In J. S. Adams, D. Feldman, & J. W. Pike (Eds.), *Vitamin D* (3rd ed., pp. 73–93). s.l.: Elsevier professional. https://doi.org/10.1016/B978-0-12-381978-9.10006-X.

Hong, I. K., Kim, S. in, & Lee, S. B. (2018). Effects of HLB value on oil-in-water emulsions: Droplet size, rheological behavior, zeta-potential, and creaming index. *Journal of Industrial and Engineering Chemistry, 67*, 123–131. https://doi.org/10.1016/j.jiec.2018.06.022

Hou, Y., Liu, H., Zhu, D., Liu, J., Zhang, C., Li, C., et al. (2022). Influence of soybean dietary fiber on the properties of Konjac Glucomannan/κ-carrageenan corn oil composite gel. *Food Hydrocolloids, 129*, Article 107602. https://doi.org/10.1016/j.foodhyd.2022.107602

Hu, X., Zhou, H., & McClements, D. J. (2022). Utilization of emulsion technology to create plant-based adipose tissue analogs: Soy-based high internal phase emulsions. *Food Structure, 33*, Article 100290. https://doi.org/10.1016/j.foostr.2022.100290

J.K. Hwang, Y.S. Kim, & Y.R. Pyun. Comparison of the effect of soy protein isolate concentration on emulsion stability in the absence or presence of monoglyceride.

Hyldig, G., & Nielsen, D. (2001). A review OF sensory and INSTRUMENTAL METHODS used to evaluate the texture OF FISH muscle. *Journal of Texture Studies, 32*(3), 219–242. https://doi.org/10.1111/j.1745-4603.2001.tb01045.x

Initiative For Responsible Carnauba. (2021). *Tackling environmental and Social Challenges through industry working groups: The case of carnauba wax from Brazil*.

International Organization for Standardization. (2009). ISO 10993-5: Biological evaluation of medical devices: Part 5: Tests for in vitro cytotoxicity. Retrieved from https://nhiso.com/wp-content/uploads/2018/05/ISO-10993-5-2009.pdf.

Jiménez-Colmenero, F., Cofrades, S., Herrero, A. M., Fernández-Martín, F., Rodríguez-Salas, L., & Ruiz-Capillas, C. (2012). Konjac gel fat analogue for use in meat products: Comparison with pork fats. *Food Hydrocolloids, 26*(1), 63–72. https://doi.org/10.1016/j.foodhyd.2011.04.007

Joung, D., Truong, V., Neitzke, C. C., Guo, S.-Z., Walsh, P. J., Monat, J. R., … McAlpine, M. C. (2018). 3d printed stem-cell derived Neural Progenitors generate Spinal Cord scaffolds. *Advanced Functional Materials, 28*(39). https://doi.org/10.1002/adfm.201801850

K Handral, H., Hua Tay, S., Wan Chan, W., & Choudhury, D. (2022). 3d Printing of cultured meat products. *Critical Reviews in Food Science and Nutrition, 62*(1), 272–281. https://doi.org/10.1080/10408398.2020.1815172

Kamlow, M.-A., Spyropoulos, F., & Mills, T. (2021). 3D printing of kappa-carrageenan emulsion gels. *Food Hydrocolloids for Health, 1*, Article 100044. https://doi.org/10.1016/j.fhfh.2021.100044

Kazir, M., & Livney, Y. D. (2021). Plant-based seafood analogs. *Molecules, 26*(6), 1559. https://doi.org/10.3390/molecules26061559

Kocatepe, D., & Turan, H. (2012). Chemical composition of cultured sea bass (Dicentrarchus labrax, Linnaeus 1758) muscle. *Journal of Food and Nutrition Research, 51*(1), 33–39.

Kouzani, A. Z., Adams, S., Whyte, D. J., Oliver, R., Hemsley, B., Palmer, S., et al. (2017). 3D printing of food for People with swallowing difficulties. *KnE Engineering, 2*(2), 23. https://doi.org/10.18502/keg.v2i2.591

Lazo, O., Guerrero, L., Alexi, N., Grigorakis, K., Claret, A., Pérez, J. A., et al. (2017). Sensory characterization, physico-chemical properties and somatic yields of five emerging fish species. *Food Research International, 100*(Pt 1), 396–406. https://doi.org/10.1016/j.foodres.2017.07.023

Li, J., Niu, R., Zhu, Q., Yao, S., Zhou, J., Wang, W., … Xu, E. (2023). Nanostarch-enhanced 3D printability of carrageenan emulsion gel for high-fidelity and nutrition-fortified fish fat mimics. *Food Hydrocolloids, 145*, Article 109099. https://doi.org/10.1016/j.foodhyd.2023.109099

Listrat, A., Lebret, B., Louveau, I., Astruc, T., Bonnet, M., Lefaucheur, L., … Bugeon, J. (2016). How muscle structure and composition influence meat and flesh quality. *TheScientificWorldJOURNAL.* , Article 3182746. https://doi.org/10.1155/2016/3182746, 2016.

Liu, S., & Li, L. (2016). Thermoreversible gelation and scaling behavior of Ca2+-induced κ-carrageenan hydrogels. *Food Hydrocolloids, 61*, 793–800. https://doi.org/10.1016/j.foodhyd.2016.07.003

Liu, Y., Zhang, W., Wang, K., Bao, Y., Regenstein, J. M., & Zhou, P. (2019). Fabrication of gel-like emulsions with whey protein isolate using Microfluidization: Rheological properties and 3D printing performance. *Food and Bioprocess Technology, 12*(12), 1967–1979. https://doi.org/10.1007/s11947-019-02344-5

Marques, D. M. C., Silva, J. C., Serro, A. P., Cabral, J. M. S., Sanjuan-Alberte, P., & Ferreira, F. C. (2022). 3d bioprinting of novel κ-carrageenan bioinks: An algae-derived polysaccharide. *Bioengineering, 9*(3). https://doi.org/10.3390/bioengineering9030109

McClements, D. J. (2007). Critical review of techniques and methodologies for characterization of emulsion stability. *Critical Reviews in Food Science and Nutrition, 47*(7), 611–649. https://doi.org/10.1080/10408390701289292

Oh, I., Lee, J., Lee, H. G., & Lee, S. (2019). Feasibility of hydroxypropyl methylcellulose oleogel as an animal fat replacer for meat patties. *Food Research International, 122*, 566–572. https://doi.org/10.1016/j.foodres.2019.01.012

Ouyang, L., Yao, R., Zhao, Y., & Sun, W. (2016). Effect of bioink properties on printability and cell viability for 3D bioplotting of embryonic stem cells. *Biofabrication, 8*(3), Article 35020. https://doi.org/10.1088/1758-5090/8/3/035020

Paglarini, C.d. S., Furtado, G.d. F., Biachi, J. P., Vidal, V. A. S., Martini, S., Forte, M. B. S., … Pollonio, M. A. R. (2018). Functional emulsion gels with potential application in meat products. *Journal of Food Engineering, 222*, 29–37. https://doi.org/10.1016/j.jfoodeng.2017.10.026

Pan, S., Sivanathan, S., Kiepe, G., Kiepe, T., & Germann, N. (2021). Candidate formulations for a sustainable lipstick supplemented with vitamin D3: Effects of wax type and concentration on material properties. *Industrial & Engineering Chemistry Research, 60*(5), 2027–2040. https://doi.org/10.1021/acs.iecr.0c05264

Paredes, J., Cortizo-Lacalle, D., Imaz, A. M., Aldazabal, J., & Vila, M. (2022). Application of texture analysis methods for the characterization of cultured meat. *Scientific Reports, 12*(1), 3898. https://doi.org/10.1038/s41598-022-07785-1

Park, S., Hong, Y., Park, S., Kim, W., Gwon, Y., Jang, K.-J., et al. (2023). Designing highly Aligned cultured meat with Nanopatterns-assisted bio-printed fat scaffolds. *Journal of Biosystems Engineering, 48*(4), 503–511. https://doi.org/10.1007/s42853-023-00208-7

Patel, A. R., Nicholson, R. A., & Marangoni, A. G. (2020). Applications of fat mimetics for the replacement of saturated and hydrogenated fat in food products. *Current Opinion in Food Science, 33*, 61–68. https://doi.org/10.1016/j.cofs.2019.12.008

Periago, M., Ayala, M., López-Albors, O., Abdel, I., Martínez, C., García-Alcázar, A., … Gil, F. (2005). Muscle cellularity and flesh quality of wild and farmed sea bass, Dicentrarchus labrax L. *Aquaculture, 249*(1–4), 175–188. https://doi.org/10.1016/j.aquaculture.2005.02.047

Petrowski, G. E. Emulsion stability and its relation to foods. Carnation Research Laboratoires, Van Nuys, California, 309–359. https://doi.org/10.1016/S0065-2628(08)60341-9.

PubChem. (2022a). Cholecalciferol. Retrieved from https://pubchem.ncbi.nlm.nih.gov/compound/Cholecalciferol.

PubChem. (2022b). Docosahexaenoic acid. Retrieved from https://pubchem.ncbi.nlm.nih.gov/compound/445580.

PubChem. (2022c). Eicosapentaenoic acid. Retrieved from https://pubchem.ncbi.nlm.nih.gov/compound/446284.

Qin, P., Wang, T., & Luo, Y. (2022). A review on plant-based proteins from soybean: Health benefits and soy product development. *Journal of Agriculture and Food Research, 7*, Article 100265. https://doi.org/10.1016/j.jafr.2021.100265

Ramachandraiah, K. (2021). Potential development of sustainable 3D-printed meat analogues: A review. *Sustainability, 13*(2), 938. https://doi.org/10.3390/su13020938

Rhein-Knudsen, N., Ale, M. T., & Meyer, A. S. (2015). Seaweed hydrocolloid production: An update on enzyme assisted extraction and modification technologies. *Marine Drugs, 13*(6), 3340–3359. https://doi.org/10.3390/md13063340

Rischer, H., Szilvay, G. R., & Oksman-Caldentey, K.-M. (2020). Cellular agriculture - industrial biotechnology for food and materials. *Current Opinion in Biotechnology, 61*, 128–134. https://doi.org/10.1016/j.copbio.2019.12.003

Samard, S., & Ryu, G.-H. (2019). A comparison of physicochemical characteristics, texture, and structure of meat analogue and meats. *Journal of the Science of Food and Agriculture, 99*(6), 2708–2715. https://doi.org/10.1002/jsfa.9438

Santos-Hernández, M., Alfieri, F., Gallo, V., Miralles, B., Masi, P., Romano, A., … Recio, I. (2020). Compared digestibility of plant protein isolates by using the INFOGEST digestion protocol. *Food Research International, 137*, Article 109708. https://doi.org/10.1016/j.foodres.2020.109708

Schmid, A., & Walther, B. (2013). Natural vitamin D content in animal products. *Advances in Nutrition, 4*(4), 453–462. https://doi.org/10.3945/an.113.003780

Shahbazi, M., Jäger, H., Chen, J., & Ettelaie, R. (2021). Construction of 3D printed reduced-fat meat analogue by emulsion gels. Part II: Printing performance, thermal, tribological, and dynamic sensory characterization of printed objects. *Food Hydrocolloids, 121*, Article 107054. https://doi.org/10.1016/j.foodhyd.2021.107054

Shi, Y., Zhang, M., & Bhandari, B. (2021). Effect of addition of beeswax based oleogel on 3D printing of potato starch-protein system. *Food Structure, 27*, Article 100176. https://doi.org/10.1016/j.foostr.2021.100176

Sigma-Aldrich. Product Specification Carnaubawax No. 3 yellow -refined: CAS Nuber 8015-86-9.

Sun, Z., Lee, S.-H., Gepner, B. D., Rigby, J., Hallman, J. J., & Kerrigan, J. R. (2021). Comparison of porcine and human adipose tissue loading responses under dynamic compression and shear: A pilot study. *Journal of the Mechanical Behavior of Biomedical Materials, 113*, Article 104112. https://doi.org/10.1016/j.jmbbm.2020.104112

Suresh, P. V., Kudre, T. G., & Johny, L. C. (2018). Sustainable Valorization of seafood processing by-product/Discard. In *Waste to Wealth* (pp. 111–139). Singapore: Springer. https://doi.org/10.1007/978-981-10-7431-8_7.

Tang, C.-H. (2017). Emulsifying properties of soy proteins: A critical review with emphasis on the role of conformational flexibility. *Critical Reviews in Food Science and Nutrition, 57*(12), 2636–2679. https://doi.org/10.1080/10408398.2015.1067594

The Good Food Institute Asia Pacific (GFI APAC). (2022). The right Ingredient for the right product: Fats. Retrieved from https://gfi-apac.org/the-right-ingredient-for-the-right-product-fats/.

Thomas, A. "Fats and fatty oils," in: Ullmann's Encyclopedia of Industrial Chemistry.

Tian, H., Wang, K., Lan, H., Wang, Y., Hu, Z., & Zhao, L. (2021). Effect of hybrid gelator systems of beeswax-carrageenan-xanthan on rheological properties and printability of litchi inks for 3D food printing. *Food Hydrocolloids, 113*, Article 106482. https://doi.org/10.1016/j.foodhyd.2020.106482

Tsuruwaka, Y., & Shimada, E. (2022). Reprocessing seafood waste: Challenge to develop aquatic clean meat from fish cells. *NPJ Science of Food, 6*(1), 7. https://doi.org/10.1038/s41538-021-00121-3

Tuomisto, H. L., & Mattos, M. J. T. de (2011). Environmental impacts of cultured meat production. *Environmental Science & Technology, 45*(14), 6117–6123. https://doi.org/10.1021/es200130u

United Nations, Department of Economic and Social Affairs, & Population Division. (2019). *World population Prospects 2019: Highlights. Statistical papers - United Nations (ser. A), population and vital Statistics Report*. New York: United Nations. https://doi.org/10.18356/13bf5476-en

Verduci, E., Di Profio, E., Cerrato, L., Nuzzi, G., Riva, L., Vizzari, G., … Peroni, D. G. (2020). Use of soy-based formulas and Cow's milk Allergy: Lights and Shadows. *Frontiers in Pediatrics, 8*, Article 591988. https://doi.org/10.3389/fped.2020.591988

Wang, C., Yan, R., Li, X., Sang, S., McClements, D. J., Chen, L., … Jin, Z. (2023). Development of emulsion-based edible inks for 3D printing applications: Pickering emulsion gels. *Food Hydrocolloids, 138*, Article 108482. https://doi.org/10.1016/j.foodhyd.2023.108482

Watters, C. A., Edmonds, C., Sloss, K., Rosner, L. S., & Leung, P. S. (2012). A cost analysis of EPA and DHA in fish, supplements and foods. Retrieved from https://www.researchgate.net/publication/268291476_A_cost_analysis_of_EPA_and_DHA_in_fish_supplements_and_foods.

Wen, Y., Che, Q. T., Kim, H. W., & Park, H. J. (2021). Potato starch altered the rheological, printing, and melting properties of 3D-printable fat analogs based on inulin emulsion-filled gels. *Carbohydrate Polymers, 269*, Article 118285. https://doi.org/10.1016/j.carbpol.2021.118285

Wolfer, T. L., Acevedo, N. C., Prusa, K. J., Sebranek, J. G., & Tarté, R. (2018). Replacement of pork fat in frankfurter-type sausages by soybean oil oleogels structured with rice bran wax. *Meat Science, 145*, 352–362. https://doi.org/10.1016/j.meatsci.2018.07.012

Xu, Y., Yu, J., Xue, Y., & Xue, C. (2023). Enhancing gel performance of surimi gels via emulsion co-stabilized with soy protein isolate and κ-carrageenan. *Food Hydrocolloids, 135*, Article 108217. https://doi.org/10.1016/j.foodhyd.2022.108217

Yegappan, R., Selvaprithiviraj, V., Amirthalingam, S., & Jayakumar, R. (2018). Carrageenan based hydrogels for drug delivery, tissue engineering and wound healing. *Carbohydrate Polymers, 198*, 385–400. https://doi.org/10.1016/j.carbpol.2018.06.086

Yen, F.-C., Glusac, J., Levi, S., Zernov, A., Baruch, L., Davidovich-Pinhas, M., … Machluf, M. (2023). Cultured meat platform developed through the structuring of edible microcarrier-derived microtissues with oleogel-based fat substitute. *Nature Communications, 14*(1), 2942. https://doi.org/10.1038/s41467-023-38593-4

Zhao, L., Zhang, M., Chitrakar, B., & Adhikari, B. (2021). Recent advances in functional 3D printing of foods: A review of functions of ingredients and internal structures. *Critical Reviews in Food Science and Nutrition, 61*(21), 3489–3503. https://doi.org/10.1080/10408398.2020.1799327

Zia, K. M., Tabasum, S., Nasif, M., Sultan, N., Aslam, N., Noreen, A., et al. (2017). A review on synthesis, properties and applications of natural polymer based carrageenan blends and composites. *International Journal of Biological Macromolecules, 96*, 282–301. https://doi.org/10.1016/j.ijbiomac.2016.11.095